

Bayesian graphical compositional regression for microbiome data

Jialiang Mao

Yuhan Chen

Li Ma

Duke University, Durham, NC

April 8, 2022

Abstract

An important task in microbiome studies is to test the existence of and give characterization to differences in the microbiome composition across groups of samples. Important challenges of this problem include the large within-group heterogeneities among samples and the existence of potential confounding variables that, when ignored, increase the chance of false discoveries and reduce the power for identifying true signals. We propose a Bayesian graphical regression strategy to overcome these issues based on a Dirichlet tree multinomial (DTM) model for compositional data, which performs a tree-based decomposition of the original problem into a series of local testing problems. Each local problem is solved with a Bayesian regression model that adjusts for covariates and group structures. A graphical structure is used for linking the local models to achieve efficient information sharing across OTUs and taxonomic levels. We conduct an extensive simulation study to investigate the performance of the approach. The results show that the method outperforms several existing approaches in a number of representative settings. We then apply our method to the American Gut data to analyze the association of dietary habits and human's gut microbiome composition in the presence of covariates, and illustrate the importance of incorporating covariates in microbiome cross-group comparison.

1 Introduction

The human microbiome is the community of numerous microbes that inhabit the human body. Understanding the microbiome can provide insights into various aspects of human health. For example, diseases such as obesity and Type 2 diabetes have been shown to be related to the gut microbiome (Turnbaugh et al., 2006; Qin et al., 2012). Wu et al. (2011) and David et al. (2014) showed that dietary nutrients are also associated with the gut microbiome. Next generation sequencing technologies provide ways of profiling the microbiome. This is typically achieved through either shotgun sequencing on the entire genomes of microbes, or through targeting a signature gene — the 16S RNA (rRNA) gene that provides barcodes of species identity. The 16S rRNA gene of the bacteria in the samples is sequenced and the sequences are clustered into operational taxonomic units (OTUs) using preprocessing pipelines such as QIIME (Caporaso et al., 2010). Traditionally, the OTUs are used as representatives of the species at 97% similarity level and form the basis of analyzing the composition of the human microbiome (Li, 2015). A typical microbiome dataset contains an OTU table representing the counts of each identified OTU in each sample along with a phylogenetic tree that encodes the evolutionary relationships among these OTUs.

One important task of microbiome studies is to compare the composition of the microbial community of groups of subjects (Hildebrandt et al., 2009; Wu et al., 2011; Qin et al., 2012; David et al., 2014). The groups could be the treatment and control group in an experiment or a retrospective study, or more generally, groups of subjects with different values of a categorical covariate. There are various methods for comparing two groups of data samples and their underlying distributions, ranging from the classic t -test and the Kolmogorov-Smirnov test to various recently developed methods (see for example Holmes et al. (2015), Soriano and Ma (2017) and Chen and Friedman (2017)). However, existing generic approaches are not designed specifically for OTU counts and are either inapplicable

or severely underpowered for microbiome compositional data. Besides the natural constraint that the samples are count data, a method that compares the microbiome compositions needs to take into account the following four features of the OTU counts: (i) high dimensionality: the number of OTUs in the study is often large, (ii) sparsity: the OTU table is typically sparse in the sense that it contains a large proportion of zero counts, (iii) complex covariance structure: the correlations among counts of different OTUs are complicated, and (iv) large overdispersions: the counts often show large within-group heterogeneities.

The multinomial distribution is a natural candidate for modeling compositional count data. Nevertheless, directly applying the multinomial distribution to the OTU counts ignores the above challenges. In an attempt to account for (iv), [La Rosa et al. \(2012\)](#) introduced the Dirichlet-multinomial (DM) distribution by putting a Dirichlet prior on the multinomial parameters. However, the DM model neglects features (i), (ii) and (iii) of OTU counts and can suffer from lack of power or invalid significance levels. Another set of approaches account for the overdispersion of the OTU counts using multivariate logistic normal distributions ([Xia et al., 2013](#); [Grantham et al., 2017](#)). In this work, we follow the DM route due to its simplicity in computation and its flexibility for incorporating phylogenetic information.

In practice, to address (ii) and (iii), [La Rosa et al. \(2012\)](#) and [Chen and Li \(2013\)](#) suggest the aggregation of OTU counts to family or class level based on phylogenetic information, thereby reducing the number of categories in the DM and improving the robustness of the study. In the testing scenario, however, different levels of aggregation can give inconsistent results ([Tang et al., 2017](#)). In more recent developments, the phylogenetic tree is directly used to guide inference as it gives a summary of the relations among the OTUs ([Wang and Zhao, 2017](#); [Tang et al., 2017](#)). Specifically, [Wang and Zhao \(2017\)](#) generalizes the DM to the Dirichlet tree multinomial (DTM) distribution in which the OTU counts are aggregated along the phylogenetic tree and a DM model is introduced to characterize the distribution of OTU counts on each internal node of the tree into the child nodes. Using DTM, the

original testing problem is transformed to a series of node-specific testing problems along the phylogenetic tree (Tang et al., 2017). This alleviates (i) and use the phylogenetic tree as a candidate for incorporating (iii). From now on, we shall refer to the original testing problem as the “*global*” problem and each node-specific testing problem as a “*local*” problem.

However, due to (ii), many interior nodes of the phylogenetic tree contain only few OTU counts and the corresponding tests may have poor statistical power. Moreover, compositional differences are often observed to cluster into “chains” along the phylogenetic tree (Tang et al., 2017). Such chains can arise in two ways: either due to a structural constraint of a DTM model — a cross-group difference at any particular node in the phylogenetic tree induces (weaker) differences in its ancestors, or as a result of the functional relatedness of OTUs in the phylogenetic tree. For these reasons, introducing dependencies among the local tests in the DTM type models can substantially improve the power of both the global and the local tests. Tang et al. (2017) proposed a strategy to incorporate such dependencies by adding up the test statistics in triplets of neighboring nodes.

Our approach aims to effectively account for the specific features of microbiome data by marrying the DTM and graphical models. On the one hand, we apply the DTM type of composition to break the global testing problem into local ones; on the other, we specify the dependency structure of the local tests by using a graphical model to borrow information among them. The two pieces can be merged with the Bayesian testing framework to give fast and interpretable inference through a suite of computational techniques including numerical integration and message passing. In addition, we show that the Bayesian test results in substantially improved power, likely due to the way the within-group variability is dealt with — integrated out rather than estimated as in existing approaches. Moreover, the Bayesian testing framework gives a full probabilistic characterization of the testing results rather than just a p -value.

We develop our Bayesian graphical test in the general case with covariates, and intro-

duce a Bayesian graphical compositional regression (BGCR) framework. It is important to incorporate covariates in the testing of cross-group difference since the effects of unadjusted potential confounders could invalidate the analysis especially in observational studies, as we will illustrate in our numerical examples. Recent works that consider the covariates in microbiome studies have focused on prediction (Tang and Nicolae, 2017) and selection of the covariates with significant associations to the OTU counts in a regression type analysis (Wang and Zhao, 2017; Wadsworth et al., 2017; Xia et al., 2013) as well as in latent factor analysis (Ren et al., 2017; Grantham et al., 2017). In contrast, our work focuses on effective cross-group comparison. Through numeric examples, we show the importance of properly addressing the challenges (i)-(iv) and incorporating potential confounders in cross-group comparison.

In Section 2, we describe our method for testing and characterizing the cross-group differences of OTU compositions. In Section 3, four representative simulation scenarios are considered to evaluate the performance of the proposed method. An application of the method to the American Gut data is shown in Section 4. Section 5 concludes.

2 Method

2.1 DM and DTM for comparing microbiome composition

In this section, we briefly review the Dirichlet-multinomial model and the Dirichlet-tree multinomial model for cross-group comparison of OTU compositions. Consider a microbiome dataset with the OTU counts of two groups of subjects on K OTUs denoted by $\Omega = \{\text{OTU}_1, \text{OTU}_2, \dots, \text{OTU}_K\} = \{\omega_1, \omega_2, \dots, \omega_K\}$. Let n_i be the number of samples in group i , $i = 1, 2$. For the j -th sample in group i , $j = 1, \dots, n_i$, let $\mathbf{y}_{ij} = (y_{ij1}, \dots, y_{ijK})$ be its OTU counts. Moreover, let $N_{ij} = \sum_{l=1}^K y_{ijl}$ be the total number of OTUs in that sample. For simplicity, let \mathbf{Y} be the OTU counts of all the samples.

[La Rosa et al. \(2012\)](#) used the Dirichlet-multinomial model (DM) to account for the within-group heterogeneity among the OTU abundances:

$$\begin{aligned} \mathbf{y}_{ij} \mid N_{ij}, \boldsymbol{\pi}_{ij} &\stackrel{\text{ind}}{\sim} \text{Multinomial}(N_{ij}, \boldsymbol{\pi}_{ij}) \\ \boldsymbol{\pi}_{ij} \mid \boldsymbol{\pi}_i &\stackrel{\text{i.i.d.}}{\sim} \text{Dirichlet}(\nu \boldsymbol{\pi}_i) \end{aligned} \quad (2.1)$$

for $i = 1, 2$, where $\boldsymbol{\pi}_i = (\pi_{i1}, \dots, \pi_{iK})$ with $\sum_{l=1}^K \pi_{il} = 1$, and $\nu > 0$ is a dispersion parameter controls the within-group variability. Under this formulation, the problem of comparing the OTU composition of the two groups is formulated as

$$H_0 : \boldsymbol{\pi}_1 = \boldsymbol{\pi}_2 \quad \text{vs} \quad H_1 : \boldsymbol{\pi}_1 \neq \boldsymbol{\pi}_2. \quad (2.2)$$

Based on method-of-moments estimates of the parameters, a generalized Wald-type test statistic with an asymptotic null distribution $\chi^2_{(K-1)}$ as $n_i \rightarrow \infty$ for $i = 1, 2$ is proposed in [La Rosa et al. \(2012\)](#). When K is large, which is typical in a microbiome dataset, this test has large degrees of freedom and is usually underpowered. One simple approach to alleviating this problem is to aggregate OTUs from the same genus and study their composition at the genus level as suggested by [Chen and Li \(2013\)](#). However, one could also aggregate the OTUs to other levels in the hierarchy of biological classification, such as the family or order level, yet different levels of aggregation can result in inconsistent testing results ([Tang et al., 2017](#)). Another limitation of DM is its induced correlations among OTUs ([Wang and Zhao, 2017](#)). It takes the OTU counts as any count data and assumes very simple and rather arbitrary correlations among them as reflected by the single dispersion parameter. This assumption is unrealistic since the OTUs have inherent and complicated relationships with each other, partly reflected in their evolutionary history summarized in a phylogenetic tree.

[Wang and Zhao \(2017\)](#) generalized the DM to the Dirichlet-tree multinomial (DTM) model by directly incorporating the phylogenetic tree in the modeling of the OTU counts

and decomposing the DM to a series of local DMs along the tree. Specifically, let \mathcal{T} be a phylogenetic tree on the K OTUs. Let \mathcal{I} denote the set of internal nodes (i.e., non-leaf nodes) of \mathcal{T} . Without loss of generality, we assume that \mathcal{T} is bifurcating, so each non-leaf node has two children. We denote each node A of \mathcal{T} by the set of its descendant OTUs. For example, $A = \{\omega_i\}$, $1 \leq i \leq K$ represents a leaf of \mathcal{T} that contains a single OTU ω_i ; $A = \Omega$ is the root containing all the OTUs. If $A \in \mathcal{I}$, let A_l, A_r be the left and right children of A . If $A \neq \Omega$, let A_p be its parent. For each $A \in \mathcal{T}$, let $y_{ij}(A) = \sum_{l \in A} y_{ijl}$, $i = 1, 2, j = 1, \dots, n_i$ be the total OTU counts in A of the j -th sample in group i . The DTM in this setup models how the counts in $A \in \mathcal{I}$ are distributed to its two children by a beta-binomial model:

$$\begin{aligned} y_{ij}(A_l) \mid y_{ij}(A), \theta_{ij}(A) &\stackrel{\text{ind}}{\sim} \text{Binomial}(y_{ij}(A), \theta_{ij}(A)) \\ \theta_{ij}(A) \mid \theta_i(A), \nu(A) &\stackrel{\text{i.i.d.}}{\sim} \text{Beta}(\theta_i(A)\nu(A), (1 - \theta_i(A))\nu(A)), \end{aligned} \quad (2.3)$$

where $\theta_{ij}(A)$ denotes the proportion of counts in node A that are distributed to its left child A_l , $\theta_i(A)$ the “group-centroid” of the $\theta_{ij}(A)$ ’s in group i , and $\nu(A)$ a precision or dispersion parameter that controls the variability of $\theta_{ij}(A)$, for $i = 1, 2, j = 1, \dots, n_i$. Let $\mathcal{L}_{BB}(\theta_i(A), \nu(A) \mid y_{ij}(A_l), y_{ij}(A_r))$ denote the likelihood of the parameters in (2.3) obtained by integrating out $\theta_{ij}(A)$, which with slightly more general notations can be written as

$$\mathcal{L}_{BB}(\theta, \nu \mid y_1, y_2) = \begin{cases} B(\theta\nu + y_1, (1 - \theta)\nu + y_2)/B(\theta\nu, (1 - \theta)\nu), & \text{if } \nu < \infty \\ \theta^{y_1}(1 - \theta)^{y_2}, & \text{if } \nu = \infty \end{cases} \quad (2.4)$$

for $y_1, y_2 \in \{0, 1, 2, \dots\}$, $\theta \in [0, 1]$ and $\nu \in (0, \infty]$, where $B(\cdot, \cdot)$ is the Beta function. It can be shown that the DM likelihood for each sample can be factorized into a series of beta-binomial likelihoods over the tree

$$\mathcal{L}_{DM}(\boldsymbol{\pi}_i, \nu \mid \mathbf{y}_{ij}) = \prod_{A \in \mathcal{I}} \mathcal{L}_{BB}(\theta_i(A), \nu(A) \mid y_{ij}(A_l), y_{ij}(A_r)) \quad (2.5)$$

provided that $\theta_i(A) = \pi_i(A_l)/\pi_i(A)$ and $\nu(A) = \nu\pi_i(A)$, where $\pi_i(A) = \sum_{l \in A} \pi_{il}$ for $A \in \mathcal{I}$ (Dennis III, 1991; Dennis, 1996). In this sense, the DTM could be seen as a generalization of the DM.

The likelihood factorization (2.5) suggests a ‘divide-and-conquer’ strategy to perform inference on $\boldsymbol{\pi}_i$. Specifically, inference problems on $\boldsymbol{\pi}_i$ could be solved equivalently by doing inference on $\{\theta_i(A) : A \in \mathcal{I}\}$, $i = 1, 2$. Tang et al. (2017) explored this relation and restated the problem in (2.2) as jointly testing

$$H_0(A) : \theta_1(A) = \theta_2(A) \quad \text{vs} \quad H_1(A) : \theta_1(A) \neq \theta_2(A), \quad (2.6)$$

for $A \in \mathcal{I}$. For each local test, the test in La Rosa et al. (2012) is adopted, each with only one degree of freedom.

In this work, we shall consider a Bayesian approach of testing, which will provide the building blocks for our graphical model that links the local tests. A Bayesian test on $H_0(A)$ vs $H_1(A)$ can be performed easily due to the conjugate nature of the beta-binomial model. Specifically, let

$$S(A) = \begin{cases} 0, & H_0(A) \text{ is true,} \\ 1, & H_1(A) \text{ is true,} \end{cases} \quad (2.7)$$

be the state indicator of the local test on node A . Let $G_A(\nu)$ be the prior on $\nu(A)$, $F_{0,A}(\theta)$ the prior on $\theta(A) = \theta_1(A) = \theta_2(A)$ under $H_0(A)$, and $F_{1,A}(\theta_i)$ the independent prior on $\theta_i(A)$ under $H_1(A)$, $i = 1, 2$. Based on (2.4), the marginal likelihoods under $H_0(A)$ and $H_1(A)$ are

$$\begin{aligned} M_0(A) &= \int \prod_{i=1}^2 \prod_{j=1}^{n_i} \mathcal{L}_{BB}(\theta, \nu \mid y_{ij}(A_l), y_{ij}(A_r)) dF_{0,A}(\theta) dG_A(\nu), \\ M_1(A) &= \int \prod_{i=1}^2 \left[\int \prod_{j=1}^{n_i} \mathcal{L}_{BB}(\theta_i, \nu \mid y_{ij}(A_l), y_{ij}(A_r)) dF_{1,A}(\theta_i) \right] dG_A(\nu). \end{aligned}$$

Based on $M_0(A)$ and $M_1(A)$, posterior inference on $S(A)$ can be performed by Bayes' theorem. We give details on the computational strategy for evaluating the marginal likelihoods and generalize this strategy to allow adjustment for covariates in the following sections.

2.2 Bayesian compositional regression for microbiome data

DM and DTM model samples from each group as variations around some group “centroid”, without explicitly modeling many other possible sources of variation among them. Recent literature has shown that many covariates have associations and possible effects on the microbiome composition (Wang and Zhao, 2017; Wadsworth et al., 2017; Xia et al., 2013; Tang and Nicolae, 2017; Ren et al., 2017; Grantham et al., 2017). In the testing scenario, ignoring relevant covariates will reduce the power for identifying differences, or worse yet, lead to false positives. Microbiome datasets often come with abundant covariates for the subjects in the study. Including some of these covariates in the test can give us an opportunity to improve the accuracy of the testing results and reduce the chance of false discoveries. For example, when the grouping variable is some dietary habits of the subjects, their disease history and alcohol intake are reasonable candidates for inclusion (Section 4).

Our approach takes the DTM route and incorporates covariates in each node-specific testing problem. We adopt this “divide-and-conquer” strategy of DTM not only for the possible statistical power gained by decomposing the original problem to a series of node-specific ones, but also for the natural way it offers to characterize the cross-group differences and to report the results. Specifically, by reporting the nodes in the phylogenetic tree on which the nulls are rejected, we could have a description of the set of microbes that are most relevant to the cross-group differences, which offers more insights than merely providing a decision about a test on the global null.

For the j -th sample in group i , let $\mathbf{x}_{ij} = (1, x_{ij1}, \dots, x_{ijp}) \in \mathbb{R}^{p+1}$ denote the p covariates

to be adjusted for and let $z_{ij} \in \{0, 1\}$ be its group indicator. For each $A \in \mathcal{I}$, let

$$\begin{aligned} y_{ij}(A_l) \mid y_{ij}(A), \theta_{ij}(A) &\stackrel{\text{ind}}{\sim} \text{Binomial}(y_{ij}(A), \theta_{ij}(A)) \\ \theta_{ij}(A) \mid \mathbf{x}_{ij}, z_{ij}, \nu(A) &\sim \text{Beta}(\theta_{\mathbf{x}_{ij}, z_{ij}}(A)\nu(A), (1 - \theta_{\mathbf{x}_{ij}, z_{ij}}(A))\nu(A)) \\ g(\theta_{\mathbf{x}_{ij}, z_{ij}}(A)) &= \mathbf{x}_{ij}^\top \boldsymbol{\beta}(A) + z_{ij}\gamma(A), \end{aligned} \quad (2.8)$$

where $g : [0, 1] \rightarrow \mathbb{R}$ is a link function, such as the logit link $g(x) = \log(x/(1-x))$ for $x \in (0, 1)$. $\boldsymbol{\beta}(A) \in \mathbb{R}^{p+1}$ and $\gamma(A) \in \mathbb{R}$ are the unknown parameters of the local model on A . Instead of modeling the OTU counts around some “group-specific centroid”, we model them around some “covariate-specific centroid” with the grouping information included as a special “covariate”. With this formulation, testing the global null is equivalent to jointly testing a set of local hypotheses on all $A \in \mathcal{I}$:

$$H_0(A) : \gamma(A) = 0 \quad \text{vs} \quad H_1(A) : \gamma(A) \neq 0. \quad (2.9)$$

To take a Bayesian approach for testing, for each local test, we first need to specify priors for $\boldsymbol{\beta}(A)$ and $\gamma(A)$. A simple choice is to put independent normal priors on the elements of $\boldsymbol{\beta}(A)$ and $\gamma(A)$. Note that using vague proper priors on the model specific parameters $\gamma(A)$ is often dangerous and would cause the so-called “Bartlett’s Paradox” when $\sigma \rightarrow \infty$ (Berger et al., 2001). Alternatively, various principles for constructing “objective” priors for the coefficients can be adopted. For example, generalizations of the g -prior and the mixture of g -priors (Liang et al., 2008) for linear regressions to GLMs can be employed here, see for example Held et al. (2015) and Li and Clyde (2015). Specifically, we could apply the local information metric (LIM) g -prior as suggested by Li and Clyde (2015) on $\gamma(A)$. In our setting, the difference in dimensions between the parameter space under the alternative and the null is only one; therefore, putting normal prior $N(0, \sigma_\gamma^2(A))$ with reasonably large variance (such as $\sigma_\gamma^2(A) = 10$) would give reasonable results. For the “common” parameters $\boldsymbol{\beta}(A)$, we adopt

independent normal priors $N(0, \sigma_{\beta}^2(A))$ with large $\sigma_{\beta}(A)$ on its elements. For example, when the covariates are standardized (rescaled to have a mean of zero and a standard deviation of one), $N(0, 16)$ covers most probable values of $\beta(A)$ in many applications.

Without further knowledge about the nuisance dispersion parameter $\nu(A)$, we put a prior $G_A(\nu)$ on it and integrate it out. This is key to the improvement gained by applying a Bayesian testing scheme compared to its frequentist counterparts that rely on a point estimator of $\nu(A)$ (Section 3). It is necessary for $G_A(\nu)$ to have a large support to allow various levels of dispersions. To this end, we take $\log_{10} \nu(A) \sim \text{Unif}(-1, 4)$, which covers a wide range of dispersion levels. Other choices with unbounded support such as Gamma priors on $\nu(A)$ can also be adopted.

To start the formulation, we again consider the state indicator $S(A)$ as in (2.7) for $A \in \mathcal{T}$. If A is a leaf of \mathcal{T} , we set $S(A) = 0$ since there is no test performed on A . Otherwise, let $S(A) \stackrel{\text{ind}}{\sim} \text{Bernoulli}(\rho(A))$ *a priori*, and consider a local hierarchical model for each $A \in \mathcal{I}$:

$$\begin{aligned}
S(A) \mid \rho(A) &\stackrel{\text{ind}}{\sim} \text{Bernoulli}(\rho(A)), \quad \nu(A) \mid G_A \stackrel{\text{ind}}{\sim} G_A \\
\beta(A) &\stackrel{\text{ind}}{\sim} N_{p+1}(\mathbf{0}, \sigma_{\beta}^2(A) \cdot I_{p+1}) \\
\gamma(A) &\stackrel{\text{ind}}{\sim} \mathbb{1}_{[S(A)=0]} \cdot \delta_0 + \mathbb{1}_{[S(A)=1]} \cdot N(0, \sigma_{\gamma}^2(A)) \\
g(\theta_{\mathbf{x}_{ij}, z_{ij}}(A)) &= \mathbf{x}_{ij}^{\top} \beta(A) + z_{ij} \gamma(A) \\
\theta_{ij}(A) \mid \mathbf{x}_{ij}, z_{ij}, \nu(A) &\sim \text{Beta}(\theta_{\mathbf{x}_{ij}, z_{ij}}(A) \nu(A), (1 - \theta_{\mathbf{x}_{ij}, z_{ij}}(A)) \nu(A)) \\
y_{ij}(A_l) \mid y_{ij}(A), \theta_{ij}(A) &\stackrel{\text{ind}}{\sim} \text{Binomial}(y_{ij}(A), \theta_{ij}(A)), \quad i = 1, 2, j = 1, \dots, n_i,
\end{aligned} \tag{2.10}$$

where I_{p+1} is the $(p + 1)$ -dimensional identity matrix, $\mathbb{1}_{[\cdot]}$ the indicator function, and δ_0 a point mass at zero. We refer to this model as a Bayesian compositional regression (BCR).

The local testing problem now becomes the inference problem on $S(A)$. Let $M_s(A)$ be

the marginal likelihood under $H_s(A)$, $s \in \{0, 1\}$. We have

$$M_s(A) = C \int \int \prod_{i=1}^2 \prod_{j=1}^{n_i} \mathcal{L}_{BB}(g^{-1}(\mathbf{x}_{ij}^\top \boldsymbol{\beta} + z_{ij}\gamma), \nu \mid y_{ij}(A_l), y_{ij}(A_r)) dF_{s,A}(\boldsymbol{\beta}) dF_{s,A}(\gamma) dG_A(\nu),$$

where C is a constant with respect to the parameters, $F_{s,A}(\boldsymbol{\beta})$, $F_{s,A}(\gamma)$ are the priors for $\boldsymbol{\beta}(A)$ and $\gamma(A)$ under $H_s(A)$, $\mathcal{L}_{BB}(\cdot)$ the beta-binomial marginal likelihood defined in (2.4), and $G_A(\nu)$ the prior on $\nu(A)$. The posterior of $S(A)$ is

$$S(A) \mid \rho(A), \nu(A) \sim \text{Bern}(\tilde{\rho}(A)), \text{ where } \tilde{\rho}(A) = \frac{\rho(A)M_1(A)}{(1 - \rho(A))M_0(A) + \rho(A)M_1(A)}.$$

We shall refer to $\tilde{\rho}(A) = \Pr(S(A) = 0 \mid \mathbf{Y})$ as the *posterior marginal alternative probability* (PMAP) on node A . The PMAP is large when the evidence against the local null is strong. The set of PMAPs along \mathcal{T} can be used to test the global null and pinpoint the signals. We postpone the details on using PMAPs for making such decisions based on multiple testing consideration in Section 2.4.

2.3 Bayesian graphical compositional regression

The above local test on node A is performed based only on the empirical evidence in A . Let $\mathcal{S} = \{S(A) : A \in \mathcal{I}\}$, the collection of all latent states on \mathcal{I} . Elements in \mathcal{S} are independent *a priori*. However, this independence assumption disregards the inherent relations of the $S(A)$'s — that they are naturally linked by the phylogenetic tree. Introducing suitable dependency structures on \mathcal{S} can enhance inference because (1) cross-group difference often occurs along the phylogenetic tree in a clustered manner, forming chains, which is pointed out in [Tang et al. \(2017\)](#) and will be confirmed in our data analysis, and (2) from a statistical perspective, some local tests may involve only few counts and their power is thus limited, especially when the nodes are close to the leaves of \mathcal{T} . Introducing a dependency structure

on \mathcal{S} allows these nodes to borrow information from each other and increases the power of the tests.

The dependency structure we introduce should satisfy two desiderata. On the one hand, it should allow flexible information sharing among nodes that are close on the phylogenetic tree. On the other hand, it should keep the posterior inference tractable.

Let G denote the graphical structure whose vertex set is \mathcal{S} . The way the series of local beta-binomial models are built suggests a natural “bottom-up” auto-regressive structure on \mathcal{S} that meets the above desiderata. Specifically, if the signal (cross-group difference) is present at a certain node $A \in \mathcal{T}$, it tends to appear in the parent node of A as well. Following this reasoning, we put an auto-regressive model on each $A \in \mathcal{I}$

$$\begin{aligned} \text{logit}[\Pr(S(A) = 1 \mid S(A_l), S(A_r))] &= \alpha(A) + \tau(A) \cdot \mathbb{1}_{[S(A_l) + S(A_r) \geq 1]} \\ &\quad + \kappa(A) \cdot \mathbb{1}_{[S(A_l) + S(A_r) = 2]}, \end{aligned} \tag{2.11}$$

where $\tau(A), \kappa(A) \geq 0$ together describe how likely signals at A are passed upwards along the tree. This model can be embedded in a family of models specified by the conditional probabilities

$$\Pr(S(A) = s \mid S(A_l) = s_l, S(A_r) = s_r) = \rho_{s_l s_r, s}(A), \tag{2.12}$$

where $s, s_l, s_r \in \{0, 1\}$ and $\rho_{s_l s_r, s} \in [0, 1]$. Specifically, the auto-regressive model forces $\rho_{01,s}(A) = \rho_{10,s}(A)$ (With no specific prior information, we do not differentiate between the two children of a node). Equivalently, the conditional probability of $S(A)$ given $S(A_l), S(A_r)$

can be characterized by the following transition matrix

$$\boldsymbol{\rho}(A) = \begin{pmatrix} \rho_{00,0}(A) & \rho_{00,1}(A) \\ \rho_{01,0}(A) & \rho_{01,1}(A) \\ \rho_{10,0}(A) & \rho_{10,1}(A) \\ \rho_{11,0}(A) & \rho_{11,1}(A) \end{pmatrix}$$

where the elements in each row of $\boldsymbol{\rho}(A)$ sum up to 1. Let $\boldsymbol{\rho} = \{\boldsymbol{\rho}(A) : A \in \mathcal{I}\}$. The auto-regressive model with $\boldsymbol{\rho}$ induces a specific undirected graph structure G on \mathcal{S} . It can be shown that $S(A_1), S(A_2)$ are connected in G if and only if A_1, A_2 are two children of a common parent or they form a parent-child pair in \mathcal{T} . [Figure 1](#) illustrates the relations in \mathcal{T} , the dependency structure induced by $\boldsymbol{\rho}$, and the corresponding undirected graph G with a fictional example. With the graphical structure introduced, we still have the hierarchical structure as in (2.10) with the first line replaced by the transitional probabilities defined in (2.12). We shall refer to this model as the Bayesian graphical compositional regression (BGCR).

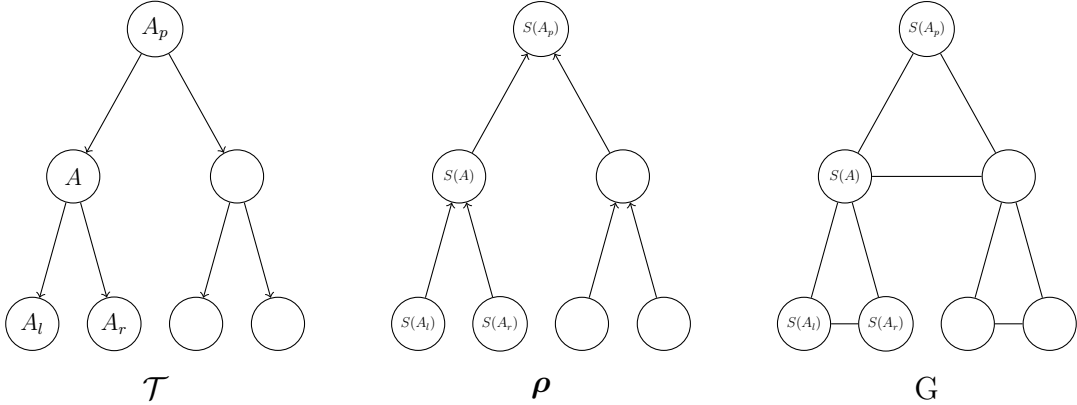


Figure 1: A phylogenetic tree and the corresponding “bottom-up” dependency structure on \mathcal{S} . The leaves of \mathcal{T} are not shown.

The choice of an auto-regressive model rather than the simpler “top-down” Markov tree model ([Crouse et al., 1998](#); [Soriano and Ma, 2017](#)) is made purposefully. In those previous

works, a “top-down” Markov tree model (MT) is introduced to the local statistics for its simplicity and amity to inference. In our setting, MT corresponds to the joint model on \mathcal{S} induced by specifying $\Pr(S(A) \mid S(A_p))$ for $A \in \mathcal{T}$. MT induces a simple tree-type dependency structure that is sparser than G and thus can give exact inference up to the approximation to the Bayes factors (Soriano and Ma, 2017). However, the “explaining away” effect (Wellman and Henrion, 1993) of the auto-regressive model is important for microbiome data. MT pushes signals downwards along the tree to both children of a node and implies cooccurrence of signals in the sibling nodes, which is not the typical situation in the microbiome context. Instead, the signals in microbiome studies often form chains, with only one of the two children nodes share the signal with the parent node. This is the primary reason for adopting a bottom-up autoregressive model.

The tree structure of MT is the key to its simple and exact inference. In contrast, the undirected graph corresponding to the bottom-up autoregressive model G contains loops of size three that break the tree structure and complicate the inference. However, the only type of loops in G is the one consisting of a node and its two children. Once we treat the three nodes in a loop together as a unit, there are no more loops in the graph and it becomes a tree. Formally, for $A \in \mathcal{I}$, we call $\mathcal{A} = \{A, A_l, A_r\}$ the *clique* of A . We also define the *clique tree* $CT(\mathcal{C})$ to be the graph with node set $\mathcal{C} = \{\mathcal{A} : A \in \mathcal{I}\}$. Two nodes $\mathcal{A}_1, \mathcal{A}_2 \in \mathcal{C}$ are connected in $CT(\mathcal{C})$ if and only if $\mathcal{A}_1 \cap \mathcal{A}_2 \neq \emptyset$. Getting back to a tree structure on the cliques retrieves the neat inference of MT. Let $S(\mathcal{A}) = (S(A), S(A_l), S(A_r))$ be the ordered triplet of the state indicators for the clique $\mathcal{A} \in \mathcal{C}$. For simplicity, we use $P = \{000, 001, 010, 011, 100, 101, 110, 111\}$ to denote the domain of $S(\mathcal{A})$. When no confusion is induced, we sometimes also use Ω to denote its clique.

For $A \in \mathcal{I}$, without loss of generality, let A be the left child of A_p . (2.12) induces the

top-down transition probabilities along the clique tree:

$$\begin{aligned}\Pr(S(\mathcal{A}) \mid S(\mathcal{A}_p)) &= \Pr(S(A), S(A_l), S(A_r) \mid S(\mathcal{A}_p), S(A), S(A_s)) \\ &= \Pr(S(A_l), S(A_r) \mid S(A)),\end{aligned}\tag{2.13}$$

for $S(\mathcal{A}) \in \mathcal{C}$. Like with $\rho(A)$, these transition probabilities could be organized into an 8×8 matrix $\xi(\mathcal{A})$:

$$\xi(\mathcal{A}) = \begin{pmatrix} \xi_{000,000} & \xi_{000,001} & \xi_{000,010} & \xi_{000,011} & \xi_{000,100} & \xi_{000,101} & \xi_{000,110} & \xi_{000,111} \\ \xi_{001,000} & \xi_{001,001} & \xi_{001,010} & \xi_{001,011} & \xi_{001,100} & \xi_{001,101} & \xi_{001,110} & \xi_{001,111} \\ \xi_{010,000} & \xi_{010,001} & \xi_{010,010} & \xi_{010,011} & \xi_{010,100} & \xi_{010,101} & \xi_{010,110} & \xi_{010,111} \\ \xi_{011,000} & \xi_{011,001} & \xi_{011,010} & \xi_{011,011} & \xi_{011,100} & \xi_{011,101} & \xi_{011,110} & \xi_{011,111} \\ \xi_{100,000} & \xi_{100,001} & \xi_{100,010} & \xi_{100,011} & \xi_{100,100} & \xi_{100,101} & \xi_{100,110} & \xi_{100,111} \\ \xi_{101,000} & \xi_{101,001} & \xi_{101,010} & \xi_{101,011} & \xi_{101,100} & \xi_{101,101} & \xi_{101,110} & \xi_{101,111} \\ \xi_{110,000} & \xi_{110,001} & \xi_{110,010} & \xi_{110,011} & \xi_{110,100} & \xi_{110,101} & \xi_{110,110} & \xi_{110,111} \\ \xi_{111,000} & \xi_{111,001} & \xi_{111,010} & \xi_{111,011} & \xi_{111,100} & \xi_{111,101} & \xi_{111,110} & \xi_{111,111} \end{pmatrix},$$

where for simplicity, we suppressed the (\mathcal{A}) 's after each element. Each row of this matrix represents the conditional distribution of $S(\mathcal{A})$ given one of the eight possible values of $S(\mathcal{A}_p)$. If \mathcal{A} is the root of \mathcal{C} , we simply let each row of $\xi(\mathcal{A})$ be the induced marginals of \mathcal{A} .

Bayesian inference on $S(\mathcal{A})$ relies on evaluating the posterior transition probability matrix $\tilde{\xi}(\mathcal{A})$ for each $\mathcal{A} \in \mathcal{C}$. We next describe how this can be achieved. For $A \in \mathcal{I}$, let $\mathcal{T}(A)$ be the subtree of \mathcal{T} with A as the root. Recall that for the j -th sample in group i , $y_{ij}(A)$ denotes the OTU counts in node A . Let $\mathbf{y}_{ij}(A)$ denote all the OTU counts that fall into the subtree $\mathcal{T}(A)$. Note that the difference between $y_{ij}(A)$ and $\mathbf{y}_{ij}(A)$ is important. $y_{ij}(A)$ contains only the counts in A while $\mathbf{y}_{ij}(A)$ contains $y_{ij}(A_d)$ for all $A_d \in \mathcal{T}(A)$. Let $\mathbf{Y}(A) =$

$\{\mathbf{y}_{ij}(A) : i = 1, 2, j = 1, \dots, n_i\}$ be the counts in $\mathcal{T}(A)$ of all the samples. Moreover, for $\mathbf{s} = (s, s_l, s_r) \in P$, let $m_{\mathbf{s}}(\mathcal{A}) = M_s(A)$. We use a recursive message-passing algorithm to calculate these posteriors. Specifically, the root of the clique tree first collect information iteratively from its children. After all the information is collected, it is distributed downwards along the tree to finish the information sharing.

Information collection. For $\mathbf{s} \in P$, let $\phi_{\mathbf{s}}(\mathcal{A})$ be the prior predictive distribution of $\mathbf{Y}(A)$ evaluated at the observed counts given $S(\mathcal{A}_p) = \mathbf{s}$. When A has children, it is given by

$$\begin{aligned}
\phi_{\mathbf{s}}(\mathcal{A}) &:= \Pr(\mathbf{Y}(A) \mid S(\mathcal{A}_p) = \mathbf{s}) \\
&= \sum_{\mathbf{s}' \in P} \Pr(\mathbf{Y}(A) \mid S(\mathcal{A}) = \mathbf{s}') \Pr(S(\mathcal{A}) = \mathbf{s}' \mid S(\mathcal{A}_p) = \mathbf{s}) \\
&= \sum_{\mathbf{s}' \in P} \xi_{\mathbf{s}, \mathbf{s}'}(\mathcal{A}) m_{\mathbf{s}'}(A) \Pr(\mathbf{Y}(\mathcal{A}_l) \mid S(\mathcal{A}) = \mathbf{s}') \Pr(\mathbf{Y}(\mathcal{A}_r) \mid S(\mathcal{A}) = \mathbf{s}') \\
&\propto \sum_{\mathbf{s}' \in P} \xi_{\mathbf{s}, \mathbf{s}'}(\mathcal{A}) m_{\mathbf{s}'}(A) \phi_{\mathbf{s}'}(\mathcal{A}_l) \phi_{\mathbf{s}'}(\mathcal{A}_r).
\end{aligned} \tag{2.14}$$

When A has no children in \mathcal{I} , by definition $\phi_{\mathbf{s}}(A) = 1$. When $A = \Omega$, \mathcal{A} does not have a parent in the clique tree. To simplify the notation and calculation, we imagine a “sentinel” node Ω_p that serves as Ω ’s parent. Without loss of generality, we let Ω be the left child of Ω_p and let Ω_s with $\phi_{\mathbf{s}}(\Omega_s) = 1$ be Ω ’s “imaginary” sibling. By setting $\Pr(S(\mathcal{A}) = \mathbf{s}' \mid S(\mathcal{A}_p) = \mathbf{s})$ to the corresponding marginals of $S(\Omega)$, we can keep the formulation in (2.14).

Information distribution. By Bayes’ theorem, the posterior transition probability

$$\begin{aligned}
\tilde{\xi}_{\mathbf{s}, \mathbf{s}'}(\mathcal{A}) &:= \Pr(S(\mathcal{A}) = \mathbf{s}' \mid S(\mathcal{A}_p) = \mathbf{s}, \mathbf{Y}(\Omega)) \\
&= \frac{\Pr(S(\mathcal{A}) = \mathbf{s}', \mathbf{Y}(\Omega) \mid S(\mathcal{A}_p) = \mathbf{s})}{\Pr(\mathbf{Y}(\Omega) \mid S(\mathcal{A}_p) = \mathbf{s})} \\
&= \frac{\Pr(S(\mathcal{A}) = \mathbf{s}' \mid S(\mathcal{A}_p) = \mathbf{s}) \Pr(\mathbf{Y}(A) \mid S(\mathcal{A}) = \mathbf{s}')}{\Pr(\mathbf{Y}(A) \mid S(\mathcal{A}_p) = \mathbf{s})} \\
&= \frac{\xi_{\mathbf{s}, \mathbf{s}'}(\mathcal{A}) m_{\mathbf{s}'}(A) \phi_{\mathbf{s}'}(\mathcal{A}_l) \phi_{\mathbf{s}'}(\mathcal{A}_r)}{\phi_{\mathbf{s}}(\mathcal{A})}.
\end{aligned} \tag{2.15}$$

Let $\tilde{\xi}(\mathcal{A})$ be the matrix of the posterior values of the transition probabilities of \mathcal{A} . Based on $\{\tilde{\xi}(\mathcal{A}) : \mathcal{A} \in CT(\mathcal{C})\}$, it is easy to compute the PMAP on each node $A \in \mathcal{T}$. Specifically, starting from the root of the tree, each row of $\tilde{\xi}(\Omega)$ represents the marginals of the clique $(\Omega, \Omega_l, \Omega_r)$. Thus

$$\Pr(S(\Omega) = \mathbf{s}' \mid \mathbf{Y}) = \sum_{\mathbf{s} \in P} \tilde{\xi}_{\mathbf{s}, \mathbf{s}'}(\Omega) / 8 \quad (2.16)$$

for $\mathbf{s}' \in P$. By marginalization, we can get the PMAP on the root node Ω . The PMAPs on other nodes can be computed by induction. For example, given the clique marginals of $S(\mathcal{A}_p)$, we can compute the clique marginals of $S(\mathcal{A})$

$$\Pr(S(\mathcal{A}) = \mathbf{s}' \mid \mathbf{Y}) = \sum_{\mathbf{s} \in P} \Pr(S(\mathcal{A}_p) = \mathbf{s} \mid \mathbf{Y}) \tilde{\xi}_{\mathbf{s}, \mathbf{s}'}(\mathcal{A}) \quad (2.17)$$

for $\mathbf{s}' \in P$, from which the PMAP on A can be obtained by marginalization. We can also compute the *posterior joint alternative probability* (PJAP) that captures the empirical evidence against the global null. Formally,

$$\text{PJAP} = 1 - \Pr(S(A) = 0, A \in \mathcal{T} \mid \mathbf{Y}) = 1 - \prod_{\mathcal{A} \in CT(\mathcal{C})} \tilde{\xi}_{\mathbf{s}_0, \mathbf{s}_0}(\mathcal{A}) \quad (2.18)$$

with $\mathbf{s}_0 = (0, 0, 0)$. Note that the above steps are a variant of the junction tree algorithm (Lauritzen and Spiegelhalter, 1988) that efficiently calculate the marginals in a graphical model. Directly applying the junction tree algorithm on $CT(\mathcal{C})$ outputs the PMAPs, however, it does not allow efficient computation of the PJAP. Algorithm 1 summarizes the entire inference recipe for testing the existence of cross-sample differences under the BGCR model.

2.4 Decision making and multiple testing control

The PJAP and the PMAPs provide the bases of making decisions about the global and the local hypotheses along the tree. Taking a decision theoretic perspective, let $d(\mathbf{y}) \in \{0, 1\}$

Algorithm 1 BGCR for comparing microbiome composition

```

for  $A$  in  $\mathcal{I}$  do ▷ Preprocessing
    Compute the marginal likelihoods of the local test on  $A$ .
    Compute the prior transition matrix  $\xi(\mathcal{A})$  on the clique of  $A$ .
    Compute  $D(A)$  — the depth of  $A$  defined as the number of edges from  $A$  to the root
    of  $\mathcal{T}$ .
end for

for  $d$  in  $\max_{A \in \mathcal{I}}\{D(A)\} : 0$  do ▷ Recursive information collection
    for  $A$  with  $D(A) = d$  do
        if  $\mathcal{A}$  has no children then
            Let  $\phi_{s'}(\mathcal{A}_l) = \phi_{s'}(\mathcal{A}_r) = 1$ ,  $s' \in P$ .
        else
            Compute  $\phi_s(\mathcal{A}) = \sum_{s' \in P} \xi_{ss'}(\mathcal{A}) m_{s'}(A) \phi_{s'}(\mathcal{A}_l) \phi_{s'}(\mathcal{A}_r)$ ,  $s \in P$ .
        end if
    end for
end for

for  $\mathcal{A}$  in  $CT(\mathcal{C})$  do ▷ Information distribution
    Compute  $\tilde{\xi}_{s,s'}(\mathcal{A}) = \frac{\xi_{s,s'}(\mathcal{A}) m_{s'}(A) \phi_{s'}(\mathcal{A}_l) \phi_{s'}(\mathcal{A}_r)}{\phi_s(\mathcal{A})}$ ,  $s, s' \in P$ .
end for

for  $d$  in  $0 : \max_{A \in \mathcal{I}}\{D(A)\}$  do ▷ Local information summary
    for  $A$  with  $D(A) = d$  do
        if  $A = \Omega$  then
            Let  $\Pr(S(\mathcal{A}) = s \mid \mathbf{Y}) = 1/8$ .
        else
            Compute  $\Pr(S(\mathcal{A}_p) = s' \mid \mathbf{Y}) = \sum_{s \in P} \Pr(S(\mathcal{A}_p) = s \mid \mathbf{Y}) \tilde{\xi}_{s,s'}(\mathcal{A})$ .
        end if
    end for
end for

Report nodes with  $\text{PMAP}(A) > c$  for some threshold  $c$ . ▷ Report significant nodes

```

be some decision rule, with $d(\mathbf{y}) = 1$ corresponding to the rejection of the global null that there are no cross-group differences in the OTU composition. When the loss function is

$$L(d(\mathbf{y}), c) = c \cdot \mathbb{1}_{[H_0 \text{ is true}]} d(\mathbf{y}) + (1 - c) \cdot \mathbb{1}_{[H_1 \text{ is true}]} (1 - d(\mathbf{y}))$$

for some $0 \leq c \leq 1$, one can show that the Bayes optimal decision rule is $d(\mathbf{y}) = \mathbb{1}_{[\text{PMAP} > c]}$. In particular, when $c = 0.5$, this gives the optimal decision under the simple 0-1 loss.

The decision on reporting the significant nodes is a multiple testing problem with dependent tests. One way to address this problem is to use loss functions specified with the false positives and false negatives (Müller et al., 2006). For example, let $d_i(\mathbf{y}) \in \{0, 1\}$ be the decision rule on the i -th node; again, $d_i(\mathbf{y}) = 1$ corresponds to the rejection of the node-specific null. Let FD and FN denote the number of false positives and false negatives. The posterior expectation of FD and FN are

$$\begin{aligned}\overline{\text{FD}} &= \sum (1 - \text{PMAP}_i) \times d_i(\mathbf{y}), \\ \overline{\text{FN}} &= \sum \text{PMAP}_i \times (1 - d_i(\mathbf{y})).\end{aligned}$$

It can be shown that under the loss $L(d(\mathbf{y}), t) = t \times \text{FD} + \text{FN}$, the Bayes optimal decision rule, which minimizes the posterior expected loss $\overline{L}(d(\mathbf{y}), t) = t \times \overline{\text{FD}} + \overline{\text{FN}}$ has the form $d_i(\mathbf{y}) = \mathbb{1}_{[\text{PMAP}_i > c']}$ with the optimal threshold $c' = t/(t + 1)$, $t \geq 0$ (Müller et al., 2004). In our application, we use $c' = 0.5$ that corresponds to $t = 1$ which is also recommended by Barbieri et al. (2004). Note that other loss functions, such as those specified with the false discovery rate (Müller et al., 2006), could also be used here.

2.5 Specifications of the hyper-parameters

In our model, we need to specify the prior transition matrix $\rho(A)$ for $A \in \mathcal{I}$, or equivalently, to specify $\alpha(A)$, $\tau(A)$ and $\kappa(A)$ in (2.11). For simplicity, we let α, τ, κ be global parameters

that are same for all $A \in \mathcal{I}$.

Choice of α . The *prior joint alternative probability* (PrJAP) can be written as

$$\text{PrJAP} = 1 - \left(\frac{1}{1 + \exp(\alpha)} \right)^{|\mathcal{I}|},$$

which is a monotone function of α . As such, we can choose $\alpha = \alpha_0$ such that the PrJAP is at a desired level such as 0.5.

Choice of κ . τ and κ together control the “stickiness” of the signals, that is, the frequency of the “chaining” pattern along the phylogenetic tree. To encapsulate the “explaining away” effect, we set $\kappa = 0$ and assume that the signal at A could be “explained away” by the signal at one of its children. Another choice for κ is $\kappa = \tau$, which imposes additive effect of signals at the sibling nodes on the parent.

Choice of τ . Given $\alpha = \alpha_0, \kappa = 0$, we use the empirical Bayes procedure to choose the value of τ . Given τ , the marginal likelihood is a byproduct of the inference procedure, equal to $\phi_s(\Omega)$ as defined in (2.14). We maximize $\phi_s(\Omega)$ over τ to get $\hat{\tau}$ as the prior choice for τ . In search of τ , we focus on the interval $[0, \tau_{max}]$, where τ_{max} is some predetermined upper bound on τ . One way to choose τ_{max} is based on the *prior marginal alternative probability* (PrMAP) on each node, which is a monotonically increasing function of τ . Therefore, the total number of nodes with PrMAP exceeding the threshold c' is also increasing with τ . This gives the total prior expected number of true alternatives. We can preselect an upper bound of this number and solve for τ_{max} . In practice, when the number of OTUs is not very large (≤ 150), we find that setting $\tau_{max} = 6$ usually works well (this corresponds to setting the prior expected sum of PrMAPs equal to 2 with 100 total OTUs). When $\tau = 0$, BGCR incorporates BCR as a special case.

3 Numerical examples

3.1 Evaluating the performance of BGCR.

We first carry out three simulation studies to illustrate the performance of the BGCR framework. The data are simulated based on the July 29, 2016 version of the fecal data of the American Gut Project (McDonald et al., 2015), which collected microbiome samples from different body sites of a large number of participants and offers publicly accessible datasets. The full dataset contains counts on 27774 OTUs of 8327 participants as well as 455 covariates describing various aspects of the subjects, such as their demographical information and dietary behaviors. A full binary phylogenetic tree on all the OTUs is also available.

Although the number of OTUs in the study is large, many cells in the OTU table contain zero counts. For illustration purpose, we focus on the top $K = 50, 75$, and 100 OTUs with the largest overall counts across samples. We further narrow down the samples to 561 middle-aged (people in their 30s, 40s and 50s) male Caucasian participants from the west census region to reduce the large variation across different simulation rounds (we will use the full dataset in our later data analysis). Reducing the size of the simulation study is also necessary due to the speed of the competitors. In each simulation scenario, we randomly divide the data into two groups with roughly equal sample size as the data under the null. The data under the alternative is generated under three scenarios:

I. Cross-group difference exists at a single OTU. This scenario is also considered in (Tang et al., 2017). In each round of the simulation, we randomly select an OTU and increase its count in the second group by a given percentage p . In this case, the group difference is considered local on the tree. We consider $K = 50, 75$, and 100 with $p = 100\%$, 150% , and 250% (To rule out obvious simulations with either too weak or too strong signals, we place additional constraints in the random selection. Specifically, we only select OTUs with sample means in the middle 80% range of all the K OTU

sample means).

II. Cross-group difference exists at multiple OTUs. Similar to the first scenario, eight OTUs are randomly selected and their counts are increased by a given percentage p of the subjects in the second group to create the case when the group difference is more global on the tree. We consider $K = 50, 75$, and 100 with $p = 50\%, 100\%$, and 150% .

III. Cross-group difference exists at a chain of nodes in the phylogenetic tree.

Cross-group differences of OTU compositions often cluster into chains as shown in [Section 4](#) and [Tang et al. \(2017\)](#). In this scenario, we create cross-group differences at a fixed chain of nodes in the phylogenetic tree. Specifically, consider a chain of three nodes in the tree ([Figure 2](#)), we increase the counts of OTU 1, 2 and 3 of all the subjects in the second group by $0.33p$, $0.67p$ and p percent, respectively. We consider the case when $K = 100$, $p = 50\%, 75\%$, and 100% .

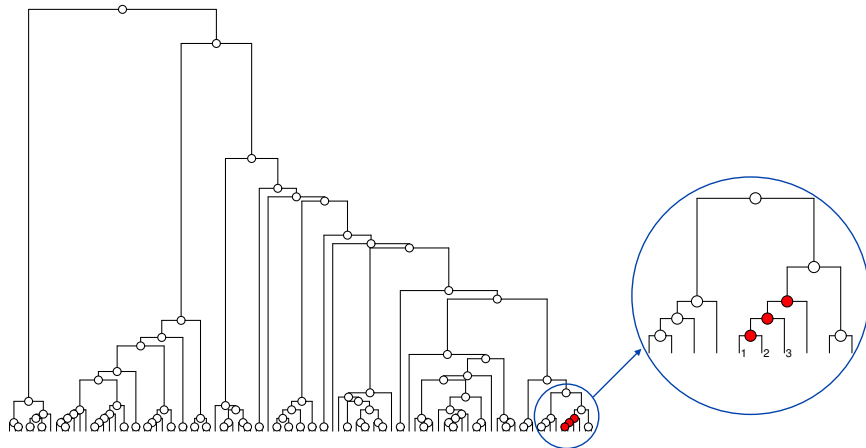


Figure 2: The chain pattern of signals in the phylogenetic tree. By construction, signals are present at the tree red nodes that form a chain.

In each scenario, we carry out 3000 rounds of simulations. For BGCR, we let $\gamma(A) \sim$

$N(0, 10)$ and $\log_{10} \nu(A) \sim \text{Unif}(-1, 4)$ independently for $A \in \mathcal{I}$. Hyperparameters are chosen according to Section 2.5 with $\text{PrJAP} = 0.5$, $\kappa = 0$, and $\tau_{max} = 6$. We compare our methods to the DTM method using the maximum of the single node statistic (DTM-1) and using the maximum of the triplet statistic (DTM-3) (Tang et al., 2017) as well as the DM test (La Rosa et al., 2012).

The ROC plots under different simulation scenarios are shown in Figure 3, Figure 4 and Figure 5. Overall, our method outperforms the competitors in all the scenarios considered. In general, the three methods that incorporate phylogenetic information perform better than the DM test. In Scenario I and II, Figure 3 and Figure 4 show that DTM-1 and DTM-3 work better when K is small. Their performance becomes worse with the increase of K . This is due to the inherent features of the microbiome data. When K is small, the samples typically contain large numbers of counts on all of the OTUs included in the study and are likely to be well described by the DM-type models. When K becomes larger, the OTU table gets sparser and the within-group heterogeneity of the OTU counts increases. Moreover, the beta-binomial model is not ideal in describing the local experiments containing OTUs with only few counts, making it harder for DTM-1 and DTM-3 to estimate the right dispersion parameters. In contrast, the dispersion parameters are integrated out rather than estimated in BGCR. Therefore, BGCR is more robust to various dispersions in the OTU counts and to possible model mis-specifications.

To illustrate how borrowing information among neighboring nodes help increase the power of the tests, we compare BGCR with BCR in Scenario III. Under the null, the estimated γ by the empirical procedure in BGCR are zero in all but a few of the simulations (Figure S1 left). Therefore, BGCR essentially degenerates to BCR and does not increase the chance of false positives (Figure S1 middle and right). Under the alternative, by introducing positive dependencies among the local tests, BGCR obtains larger PJAPs thus provides a better chance to correctly reject the null. To see how this would influence the decision procedure,

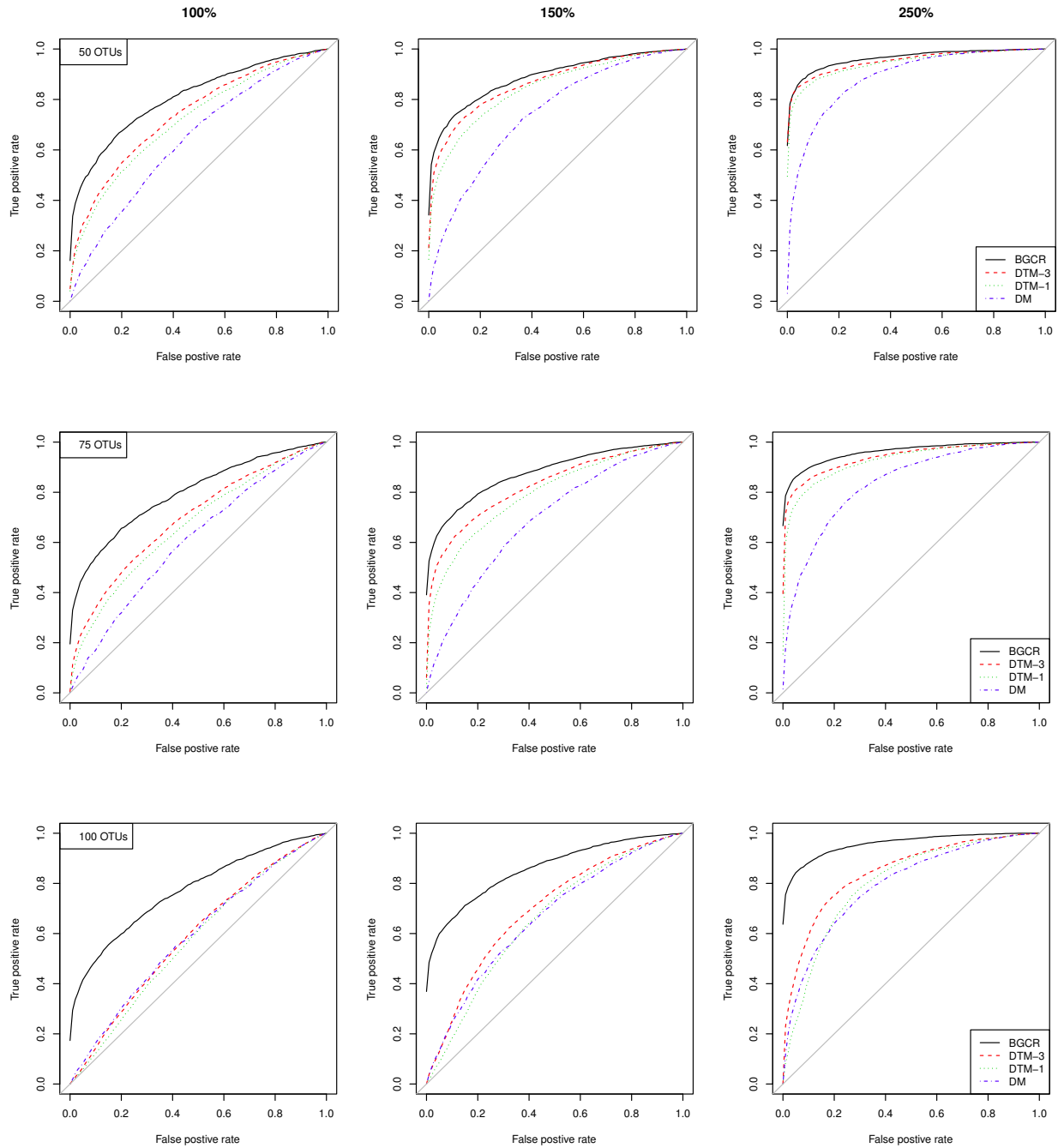


Figure 3: ROC curves for Scenario I. The rows are indicated by the total number of OTUs considered. The columns are indicated by the percent of count increased in the second group: 100% (left), 150% (middle), 250% (right).

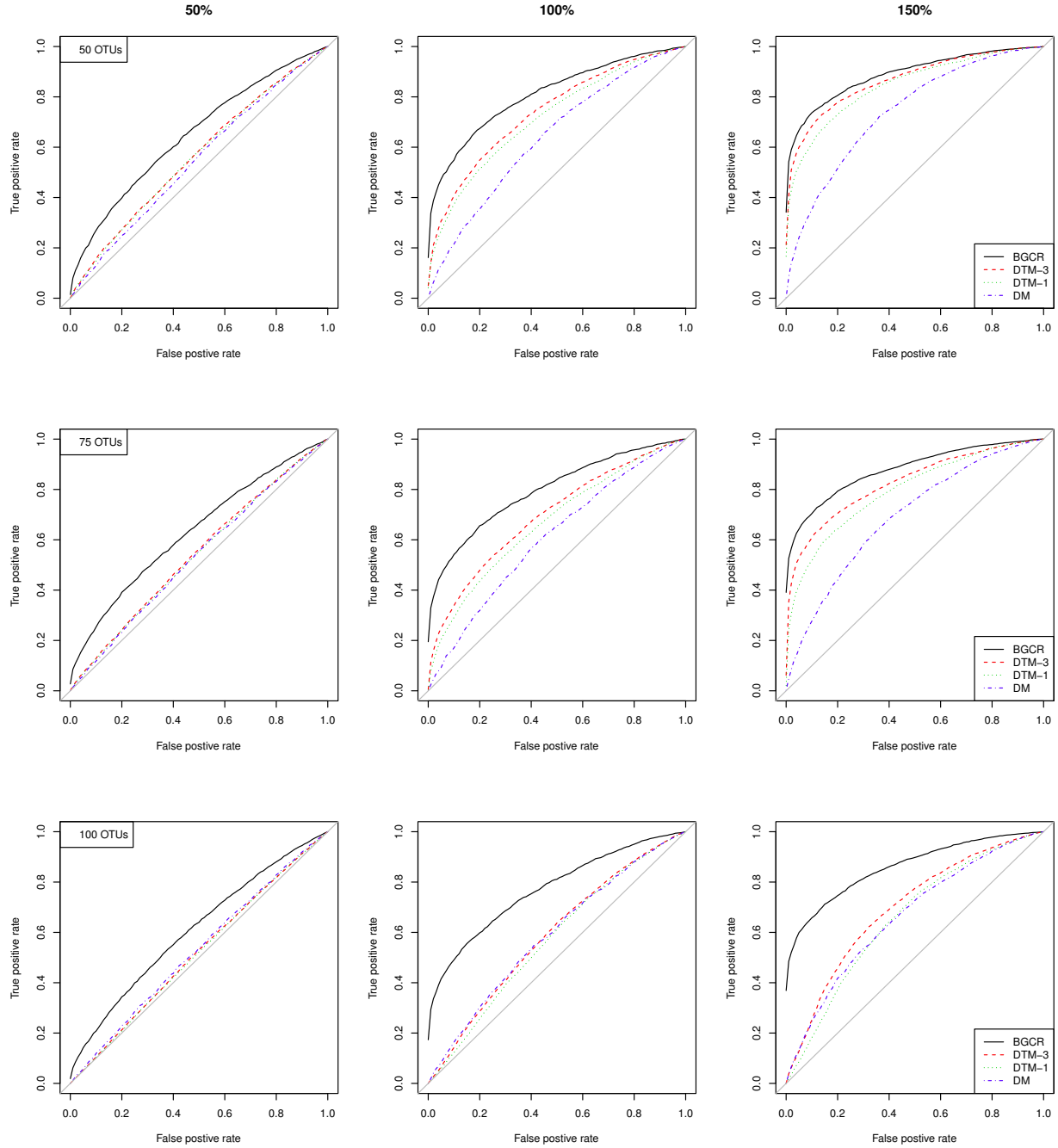


Figure 4: ROC curves for Scenario II. The rows are indicated by the total number of OTUs considered. The columns are indicated by the percent of count increased in the second group: 50% (left), 100% (middle), 150% (right).

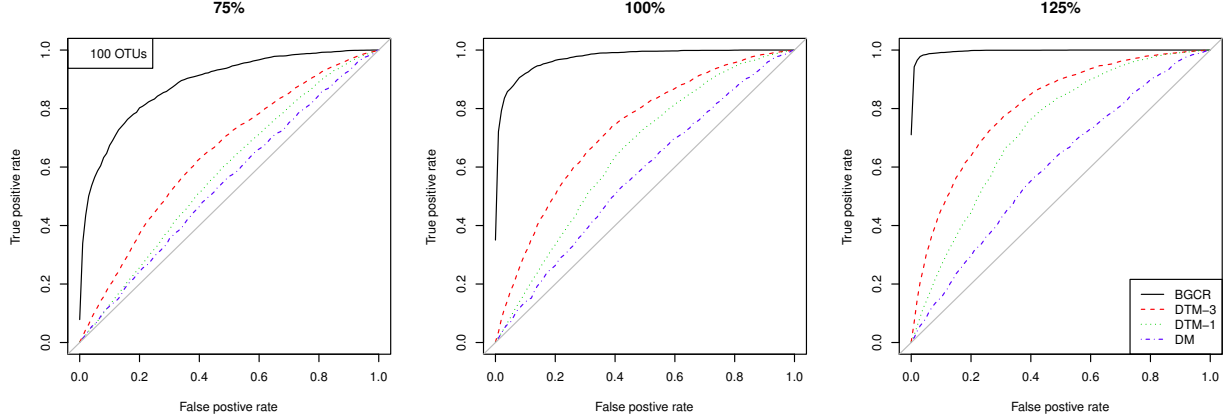


Figure 5: ROC curves for Scenario III. The columns are indicated by the percent of count increased in the second group: 75% (left), 100% (middle), 125% (right).

we show the proportion of the tests that reject the null under different decision thresholds c in Figure 6. When $0.5 < c < 0.9$, the gain by introducing the dependencies among tests is remarkable. Figure S2 shows the estimated γ 's under the alternatives. When the cross-group difference increases, the chain pattern gets stronger, causing the estimated γ to increase. Figure S3 shows the corresponding PJAPs of the two models under comparison.

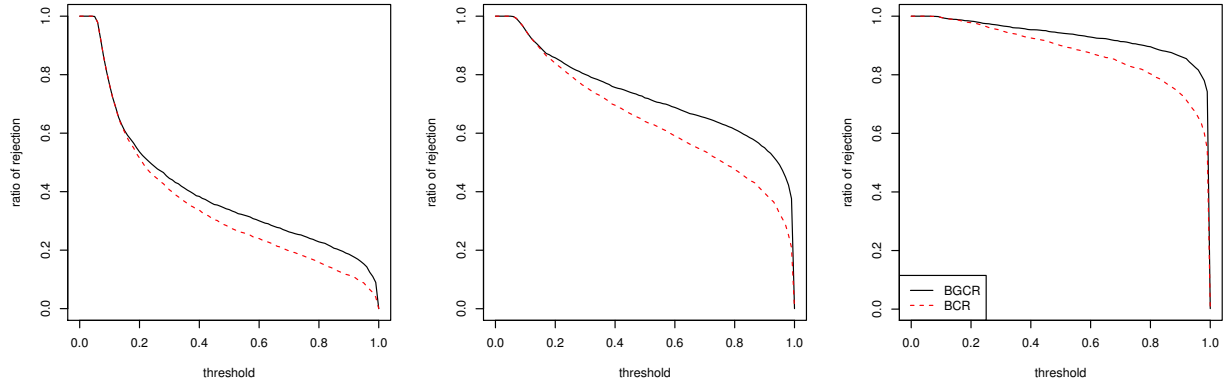


Figure 6: Ratio of rejection under the alternatives in Scenario III.

3.2 Characterizing the cross-group differences with BGCR.

In many applications, characterizing the cross-group differences is often of more interest than merely testing the existence of them. Within our Bayesian testing framework, this can be simply achieved by reporting the PMAPs of the local tests along the phylogenetic tree. Plotting the PMAPs on the tree provides a natural way to visualize the cross-group differences. [Figure 7](#) shows an example from scenario 3. In this example, $PJAP_{BGCR} = 0.910$, $PJAP_{BCR} = 0.651$, $\hat{\gamma} = 5.521$. BGCR benefits from the graphical structure and recovers the chain pattern of the signals as shown in [Figure 2](#).

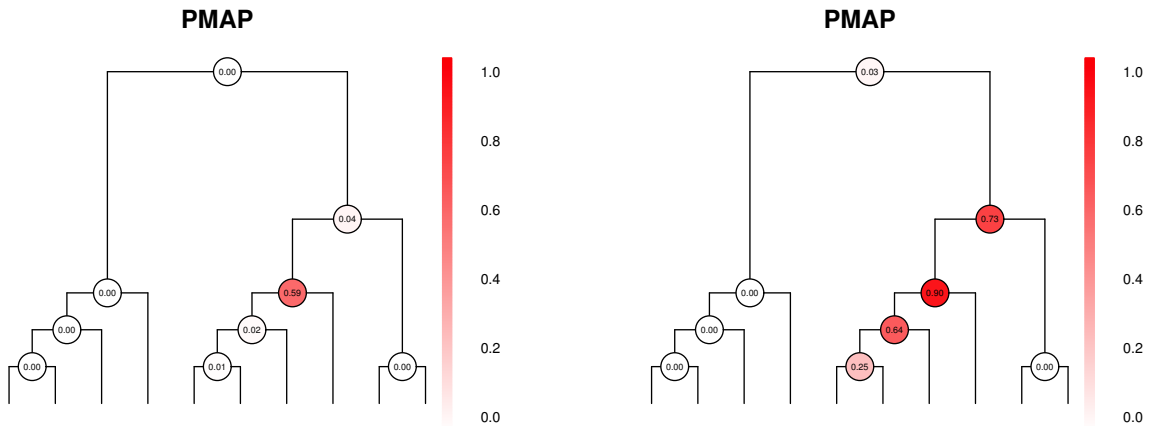


Figure 7: Characterizing the cross-group differences with the PMAPs (only shown for the zoomed in subtree in [Figure 2](#)). Left: BCR; Right: BGCR.

3.3 Adjusting for covariates.

In practice, the OTU composition can depend on various factors. When the data are gathered from observational studies instead of randomized experiments, as in the American Gut study, unadjusted covariates can lead to false positives. Even when the data do arise from randomized experiments, incorporating relevant covariates can substantially improve the power

to identify cross-group differences. We consider another simulation scenario to illustrate the necessity of incorporating confounders in the testing procedure:

IV. Cross-group difference exists at a single OTU with an unbalanced confounder. We start from the same American Gut dataset as in the previous scenarios. Instead of focusing on middle-aged *male* Caucasians from the west region, we randomly select 200 *male* and 200 *female* Caucasians, all middle aged and from the west region (the reason we take a random sample instead of using the full dataset is the large computational burden brought by the competitors). To purposefully make gender a confounder, we select an OTU (OTU ‘4352657’) and increase the counts of this OTU for all male participants by 175%. We then randomly select 160 males and 40 females into the first group and put the rest into the second group to form the data under the null. Note that the confounder “gender” is by design unbalanced in the two groups. To simulate data under the alternative, we select another OTU (OTU ‘4481131’) and increase the count of this OTU in the second group by 175%.

We carry out 750 simulations with $K = 50$ (we do not simulate 3000 rounds or consider $K = 75$ or 100 since some competitors are very slow). [Figure 8](#) shows the histograms of the relevant statistics under the null for different methods (for DTM-3, we use the PhyloScan method in [Tang et al. \(2017\)](#) to get upper bounds of the p -values). Without adjusting for the gender of the participants, all the methods fail in controlling false positives.

Adjusting for confounders is also important in the characterization of the cross-group differences. [Figure 9](#) shows an example in scenario 4. The PJAPs reported by BGCR are closed to 1 with or without “gender” in the model. However, ignoring the confounder contaminates the pattern of the cross-group differences as expected.

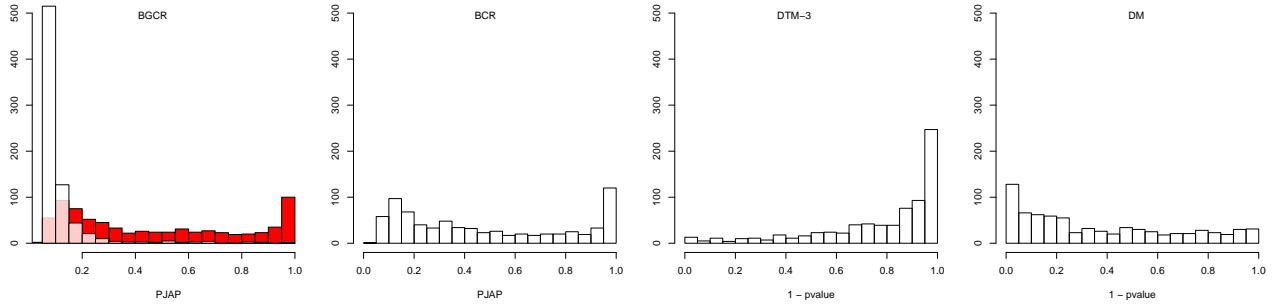


Figure 8: Control of false positives under the null when confounders exist. The histogram of the PJAPs under the alternative of BGCR with covariate adjusted is shown in red in the first plot.

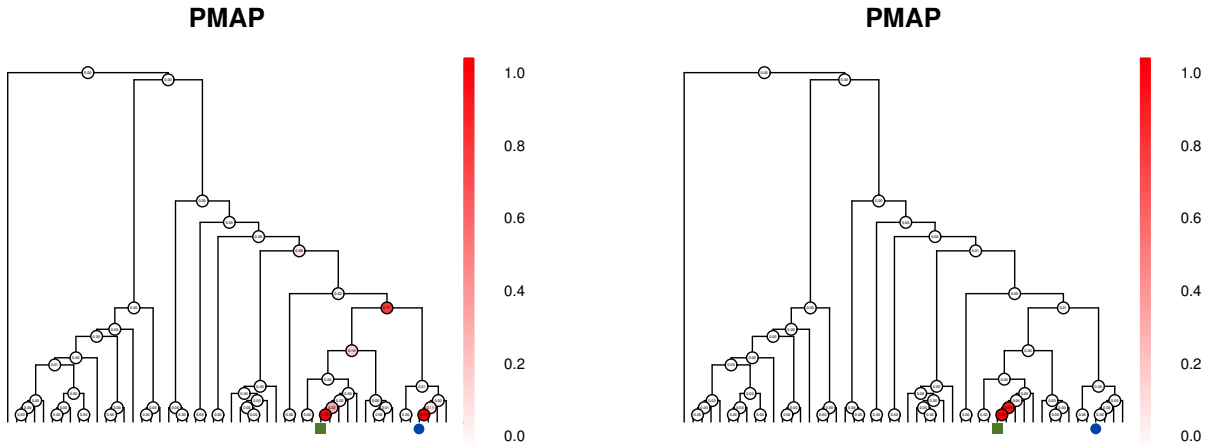


Figure 9: Characterizing the cross-group difference with the PMAPs. Left: ignoring “gender”; Right: adjusting for “gender”. The green square shows the OTU modified in the second group (true signal); the blue circle represents the OTU modified for males (false signal due to confounding with gender).

4 Application to the American Gut project

In this section, we apply BGCR to the same American Gut dataset as in [Section 3](#) focusing on the top 100 OTUs with the largest overall counts to compare the OTU composition of groups of participants with different dietary habits. The diets we considered are shown in

Table 1. For each diet, the dataset records each participant’s frequency of consumption into a categorical variable with five categories: *Never*, *Occasionally (1-2 times per week)*, *Rarely (less than once per week)*, *Regularly (3-5 times per week)* and *Daily*. We dichotomize the categories based on whether the diet is consumed less than 3 times per week and use this binary variable to divide the samples into two groups.

Besides diet, there are other possible factors that could change the OTU composition. Including these factors in the model could help reduce the chance of false discoveries and improve the power of the inference. In our analysis, we consider five such covariates: *the participant’s biological sex*, *has the participant been diagnosed with diabetes*, *does the participant have IBD (inflammatory bowel disease)*, *has the participant used antibiotic in the past year*, and *does the participant consume probiotic less than 3 times per week*. All five covariates are binary. Besides these non-dietary covariates, when investigating each dietary habit, all other dietary habits are natural candidates of confounders to be adjusted for. **Figure 10** shows an example of the unbalancedness of some diets in the two groups defined by *fruit consumption*. Therefore, we also include them in our analysis. For simplicity, we remove all the participants with missing values in any variables mentioned above and perform a complete-case analysis. We also focus on participants with age in range $20 \sim 69$ and BMI $18.5 \sim 30$ to disregard potential outliers. The sample size in each comparison is shown in **Table 1**.

For each diet, we use BGCR to compare the OTU composition of the two groups with different covariates adjusted. For comparison, we start with no covariate, and then we adjust for the five possible non-dietary confounders, and finally we adjust for the non-dietary confounders as well as other dietary habits.

Table 1 shows the PJAPs of all three methods when using each diet type as the grouping variable. When all the covariates are adjusted, the test rejects the global null under threshold $c = 0.5$ when the diet is *fruit*, *seafood*, *vegetable* or *whole grain*. For *diary* and *sweet*, adjusting

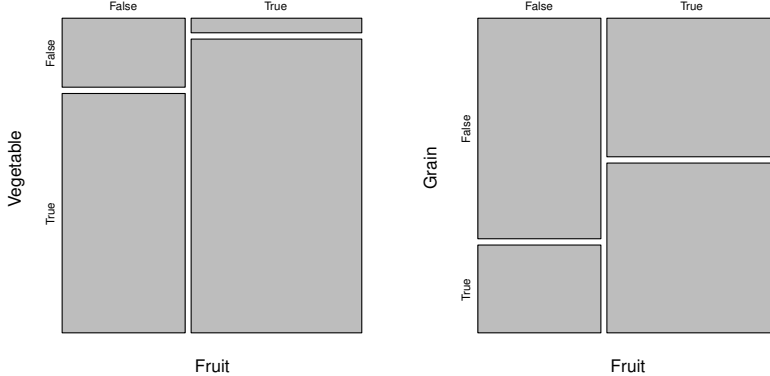


Figure 10: Unbalancedness of dietary covariates in the two groups defined by fruit consumption. The area of each block represents the counts in the corresponding cell of the 2×2 contingency table.

for the dietary covariates dramatically changes the inference. [Figure 11](#) shows the PMAPs of the four diets that are strongly related to the OTU composition. For comparison, [Figure S4](#) and [Figure S5](#) in the supplementary materials illustrate the PMAPs when no covariates or only non-dietary covariates are adjusted. Therefore, adjusting for the covariates not only changes the decision but also the characterization of the cross-group differences. For *fruit*, *vegetable* and *grain*, the estimated $\hat{\tau}$ are positive, suggesting the existence of chains of cross-group differences along the phylogenetic tree, which could also be affirmed in [Figure 11](#).

5 Concluding remarks

We have introduced a Bayesian framework for testing the existence of cross-group differences in the OTU composition. The global testing problem is transformed into a series of dependent local tests linked by the phylogenetic tree. A key feature of the Bayesian formulation is that the dispersion parameters are integrated out, providing more robust inference than the methods that use point estimates of the within-group variation. We use numerical integration

Diet	Group size		PJAP		
	False	True	No cov	Non-diet cov	All cov ($\hat{\tau}$)
Alcohol	2099	995	0.866	0.655	0.445 (0)
Diary	1733	1361	0.987	0.930	0.483 (0)
Fruit	1296	1798	> 0.999	> 0.999	0.741 (3.927)
Meat/Egg	798	2296	0.133	0.143	0.243 (0)
Seafood	2637	457	0.980	0.991	0.834 (0)
Sweets	2005	1089	0.800	0.653	0.088 (0)
Vegetable	375	2719	> 0.999	> 0.999	> 0.999 (5.132)
Whole grain	1735	1359	> 0.999	> 0.999	> 0.999 (5.626)

Table 1: PJAPs for testing OTU composition of different dietary habits. In the last column, red cells indicate rejections of the global null under threshold $c = 0.5$. The estimated $\hat{\tau}$ is shown in the parentheses.

to evaluate the Bayes factors, circumventing MCMC to give fast inference. By introducing dependencies among the local tests, information sharing is allowed among neighboring nodes. This further improves the power of the test when the cross-group differences cluster into chains along the tree, which is often observed in practice. We use an exact message passing algorithm that is scalable to the size of the tree to carry out inference under this information borrowing.

Because microbiome data often come with relevant covariates, it is important to incorporate the covariate effects. The adjustment for possible confounders during the testing procedure reduces the chance of false discoveries and the residual overdispersion. Our model achieves this by incorporating the covariates via a regression model, which adds little computational burdens to the Bayesian testing framework.

Besides testing, our model gives a full probabilistic characterization of the cross-group differences that can be naturally visualized. Note that although we focus on two group comparisons in this paper, the proposed method can be generalized to multiple group settings with little extra efforts.

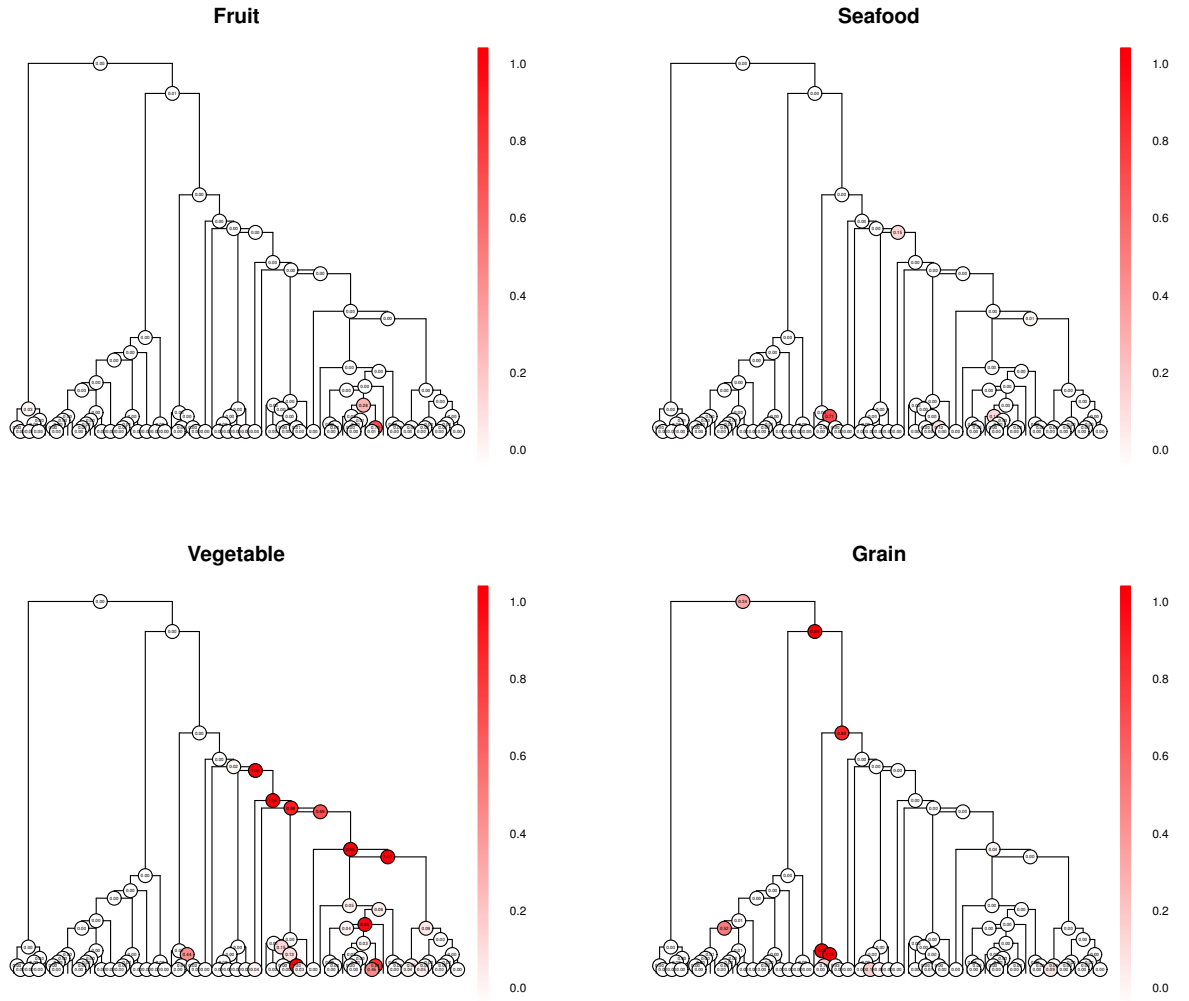


Figure 11: PMAPs for the grouping diets with rejected global null when all the covariates are adjusted.

Software

The DTM methods and the DM test are implemented with the R packages `PhyloScan` and `HMP`. R code for BGCR is freely available at <https://github.com/MaStatLab/BGCR>.

Acknowledgment

LM's research is partly supported by NSF grant DMS-1612889 and a Google Faculty Research Award.

References

Barbieri, M. M., J. O. Berger, et al. (2004). Optimal predictive model selection. *The annals of statistics* 32(3), 870–897.

Berger, J. O., L. R. Pericchi, J. Ghosh, T. Samanta, F. De Santis, J. Berger, and L. Pericchi (2001). Objective bayesian methods for model selection: introduction and comparison. *Lecture Notes-Monograph Series*, 135–207.

Caporaso, J. G., J. Kuczynski, J. Stombaugh, K. Bittinger, F. D. Bushman, E. K. Costello, N. Fierer, A. G. Peña, J. K. Goodrich, J. I. Gordon, et al. (2010). Qiime allows analysis of high-throughput community sequencing data. *Nature methods* 7(5), 335–336.

Chen, H. and J. H. Friedman (2017). A new graph-based two-sample test for multivariate and object data. *Journal of the American statistical association* 112(517), 397–409.

Chen, J. and H. Li (2013). Variable selection for sparse dirichlet-multinomial regression with an application to microbiome data analysis. *The annals of applied statistics* 7(1).

Crouse, M. S., R. D. Nowak, and R. G. Baraniuk (1998). Wavelet-based statistical signal processing using hidden markov models. *IEEE Transactions on signal processing* 46(4), 886–902.

David, L. A., C. F. Maurice, R. N. Carmody, D. B. Gootenberg, J. E. Button, B. E. Wolfe, A. V. Ling, A. S. Devlin, Y. Varma, M. A. Fischbach, et al. (2014). Diet rapidly and reproducibly alters the human gut microbiome. *Nature* 505(7484), 559–563.

Dennis, S. Y. (1996). A bayesian analysis of tree-structured statistical decision problems. *Journal of statistical planning and inference* 53(3), 323–344.

Dennis III, S. Y. (1991). On the hyper-dirichlet type 1 and hyper-liouville distributions. *Communications in Statistics-Theory and Methods* 20(12), 4069–4081.

Grantham, N. S., B. J. Reich, E. T. Borer, and K. Gross (2017). Mimix: a bayesian mixed-effects model for microbiome data from designed experiments. *arXiv preprint arXiv:1703.07747*.

Held, L., D. S. Bové, I. Gravestock, et al. (2015). Approximate bayesian model selection with the deviance statistic. *Statistical Science* 30(2), 242–257.

Hildebrandt, M. A., C. Hoffmann, S. A. Sherrill-Mix, S. A. Keilbaugh, M. Hamady, Y.-Y. Chen, R. Knight, R. S. Ahima, F. Bushman, and G. D. Wu (2009). High-fat diet determines the composition of the murine gut microbiome independently of obesity. *Gastroenterology* 137(5), 1716–1724.

Holmes, C. C., F. Caron, J. E. Griffin, D. A. Stephens, et al. (2015). Two-sample bayesian nonparametric hypothesis testing. *Bayesian Analysis* 10(2), 297–320.

La Rosa, P. S., J. P. Brooks, E. Deych, E. L. Boone, D. J. Edwards, Q. Wang, E. Sodergren, G. Weinstock, and W. D. Shannon (2012). Hypothesis testing and power calculations for taxonomic-based human microbiome data. *PLoS one* 7(12), e52078.

Lauritzen, S. L. and D. J. Spiegelhalter (1988). Local computations with probabilities on graphical structures and their application to expert systems. *Journal of the Royal Statistical Society. Series B (Methodological)*, 157–224.

Li, H. (2015). Microbiome, metagenomics, and high-dimensional compositional data analysis. *Annual Review of Statistics and Its Application* 2, 73–94.

Li, Y. and M. A. Clyde (2015). Mixtures of g-priors in generalized linear models. *arXiv preprint arXiv:1503.06913*.

Liang, F., R. Paulo, G. Molina, M. A. Clyde, and J. O. Berger (2008). Mixtures of g priors for bayesian variable selection. *Journal of the American Statistical Association* 103(481), 410–423.

Ma, L. and J. Soriano (2017). Analysis of distributional variation through multi-scale beta-binomial modeling. *arXiv preprint arXiv:1604.01443*.

McDonald, D., M. Hornig, C. Lozupone, J. Debelius, J. A. Gilbert, and R. Knight (2015). Towards large-cohort comparative studies to define the factors influencing the gut microbial community structure of asd patients. *Microbial ecology in health and disease* 26.

Müller, P., G. Parmigiani, and K. Rice (2006). Fdr and bayesian multiple comparisons rules.

Müller, P., G. Parmigiani, C. Robert, and J. Rousseau (2004). Optimal sample size for multiple testing: the case of gene expression microarrays. *Journal of the American Statistical Association* 99(468), 990–1001.

Qin, J., Y. Li, Z. Cai, S. Li, J. Zhu, F. Zhang, S. Liang, W. Zhang, Y. Guan, D. Shen, et al. (2012). A metagenome-wide association study of gut microbiota in type 2 diabetes. *Nature* 490(7418), 55–60.

Ren, B., S. Bacallado, S. Favaro, T. Vatanen, C. Huttenhower, and L. Trippa (2017). Bayesian nonparametric mixed effects models in microbiome data analysis. *arXiv preprint arXiv:1711.01241*.

Soriano, J. and L. Ma (2017). Probabilistic multi-resolution scanning for two-sample differences. *Journal of the Royal Statistical Society: Series B (Statistical Methodology)* 79(2), 547–572.

Tang, Y., L. Ma, and D. L. Niclaoe (2017). A phylogenetic scan test on dirichlet-tree multinomial model for microbiome data. *arXiv preprint arXiv:1610.08974v2*.

Tang, Y. and D. L. Nicolae (2017). Mixed effect dirichlet-tree multinomial for longitudinal microbiome data and weight prediction. *arXiv preprint arXiv:1706.06380*.

Turnbaugh, P. J., R. E. Ley, M. A. Mahowald, V. Magrini, E. R. Mardis, and J. I. Gordon (2006). An obesity-associated gut microbiome with increased capacity for energy harvest. *nature* 444(7122), 1027–131.

Wadsworth, W. D., R. Argiento, M. Guindani, J. Galloway-Pena, S. A. Shelburne, and M. Vannucci (2017). An integrative bayesian dirichlet-multinomial regression model for the analysis of taxonomic abundances in microbiome data. *BMC bioinformatics* 18(1), 94.

Wang, T. and H. Zhao (2017). A dirichlet-tree multinomial regression model for associating dietary nutrients with gut microorganisms. *Biometrics*.

Wellman, M. P. and M. Henrion (1993). Explaining'explaining away'. *IEEE Transactions on Pattern Analysis and Machine Intelligence* 15(3), 287–292.

Wu, G. D., J. Chen, C. Hoffmann, K. Bittinger, Y.-Y. Chen, S. A. Keilbaugh, M. Bewtra, D. Knights, W. A. Walters, R. Knight, et al. (2011). Linking long-term dietary patterns with gut microbial enterotypes. *Science* 334(6052), 105–108.

Xia, F., J. Chen, W. K. Fung, and H. Li (2013). A logistic normal multinomial regression model for microbiome compositional data analysis. *Biometrics* 69(4), 1053–1063.

Supplementary Materials

A Computational strategies

The crux of doing inference with BCR is to calculate the marginal likelihoods $M_s(A)$. We use the computational strategies in [Ma and Soriano \(2017\)](#) to compute the integrals. Specifically, for fixed ν , the inner integrals on the regression parameters are evaluated based on Laplace approximation; then the outer integral on ν is calculated with finite Riemann approximation.

With a bit abuse of the notations, in this section, we use $\beta(A)$ to denote the ‘active’ regression coefficient in (2.10). That is, under the null, $\beta(A)$ is just the $\beta(A)$ in (2.10); under the alternative, $\beta(A)$ denotes $(\beta(A)^\top, \gamma(A))^\top$. \mathbf{x}_{ij} is redefined to be the ‘active’ covariates in the same sense. With these notations, we have $g(\theta_{\mathbf{x}_{ij}}(A)) = \mathbf{x}_{ij}^\top \beta(A)$ and $\theta_{ij}(A) | \mathbf{x}_{ij}, \nu(A) \sim \text{Beta}(\theta_{\mathbf{x}_{ij}}(A)\nu(A), (1-\theta_{\mathbf{x}_{ij}}(A))\nu(A))$ for each local beta-binomial model.

The computational strategies are the same under both hypotheses. Let $\pi_A(\beta)$ be the prior density of $\beta(A)$ under either hypothesis. For fixed ν in the support of $G_A(\nu)$, by the Laplace approximation, the inner integral is

$$\begin{aligned}
L_\nu(A) &= \int \prod_{i=1}^2 \prod_{j=1}^{n_i} \mathcal{L}_{BB}(g^{-1}(\mathbf{x}_{ij}^\top \beta), \nu | y_{ij}(A_l), y_{ij}(A_r)) \pi_A(\beta) d\beta \\
&= \int \exp \left\{ \sum_{i,j} \log \mathcal{L}_{BB}(g^{-1}(\mathbf{x}_{ij}^\top \beta), \nu | y_{ij}(A_l), y_{ij}(A_r)) + \log \pi_A(\beta) \right\} d\beta \\
&= \int \exp \{h_\nu(\beta)\} d\beta \\
&\approx \exp \left\{ h_\nu(\hat{\beta}_\nu) \right\} \cdot (2\pi)^{d/2} \cdot | -H_\nu(\hat{\beta}_\nu)|^{-1/2} \\
&= \hat{L}_\nu(A)
\end{aligned}$$

where $h_\nu(\beta) = \sum_{i,j} \log \mathcal{L}_{BB}(g^{-1}(\mathbf{x}_{ij}^\top \beta), \nu | y_{ij}(A_l), y_{ij}(A_r)) + \log \pi_A(\beta)$, $\hat{\beta}_\nu$ is the maximizer of $h_\nu(\beta)$, $H_\nu(\hat{\beta}_\nu)$ is the Hessian matrix of $h_\nu(\beta)$ at $\beta = \hat{\beta}_\nu$. d is the degrees of freedom of β , which is $(p+2)$ under the alternative and $(p+1)$ under the null. We describe a Newton-

Raphson algorithm to solve for $\hat{\beta}_\nu$ below. The log-likelihood function is strictly log-concave and the Newton-Raphson method generally converges after only a few iterations. Finally, to get $M_s(A)$, we compute the outer integral on ν , $\int L_\nu(A) dG_A(\nu)$, with finite Riemann approximations. Specifically, after calculating $\hat{L}_\nu(A)$ at a grid of ν 's: $\nu_1, \nu_2, \dots, \nu_M$, we have

$$\int L_\nu(A) dG_A(\nu) \approx \sum_{m=2}^M \hat{L}_{\nu_m}(A)(G_A(\nu_m) - G_A(\nu_{m-1})).$$

Newton-Rhaphson for $\hat{\beta}_\nu$. In this subsection, we shall fix our attention on a specific node A and suppress the '(A)' in the notations. Moreover, we let $y_{ij}(A_l) = t_{ij}$ for simplicity and express the local Beta-Binomial regression model on A as

$$t_{ij} \sim \text{Binomial}(y_{ij}, \theta_{ij}), \quad \theta_{ij} \sim \text{Beta}(\theta_{\mathbf{x}_{ij}}\nu, (1 - \theta_{\mathbf{x}_{ij}})\nu), \quad \text{and} \quad g(\theta_{\mathbf{x}}) = \mathbf{x}^\top \boldsymbol{\beta}.$$

The contribution to the log marginal likelihood from the j -th observation in group i is

$$\begin{aligned} l_{ij} &= \log \mathcal{L}_{BB}(g^{-1}(\mathbf{x}_{ij}^\top \boldsymbol{\beta}), \nu \mid t_{ij}, y_{ij} - t_{ij}) \\ &= \log \Gamma(\theta_{\mathbf{x}_{ij}}\nu + t_{ij}) + \log \Gamma((1 - \theta_{\mathbf{x}_{ij}})\nu + y_{ij} - t_{ij}) - \log \Gamma(\nu + y_{ij}) \\ &\quad - \log \Gamma(\theta_{\mathbf{x}_{ij}}\nu) - \log \Gamma((1 - \theta_{\mathbf{x}_{ij}})\nu) + \log \Gamma(\nu). \end{aligned}$$

Taking the first derivative w.r.t. $\boldsymbol{\beta}$,

$$\frac{\partial l_{ij}}{\partial \boldsymbol{\beta}} = \frac{\partial l_{ij}}{\partial \theta_{\mathbf{x}_{ij}}} \cdot \frac{\partial \theta_{\mathbf{x}_{ij}}}{\partial \eta_{ij}} \cdot \frac{\partial \eta_{ij}}{\partial \boldsymbol{\beta}}$$

where $\eta_{ij} = \mathbf{x}_{ij}^\top \boldsymbol{\beta}$. Now with ϕ denoting the digamma function,

$$\frac{\partial l_{ij}}{\partial \theta_{\mathbf{x}_{ij}}} = \nu[\phi(\theta_{\mathbf{x}_{ij}}\nu + t_{ij}) - \phi((1 - \theta_{\mathbf{x}_{ij}})\nu + y_{ij} - t_{ij}) - \phi(\theta_{\mathbf{x}_{ij}}\nu) + \phi((1 - \theta_{\mathbf{x}_{ij}})\nu)].$$

With the logit link, $\theta_{\mathbf{x}_{ij}} = g^{-1}(\eta_{ij}) = 1/(1 + e^{-\eta_{ij}})$, and

$$\frac{\partial \theta_{\mathbf{x}_{ij}}}{\partial \eta_{ij}} = (g^{-1})'(\eta_{ij}) = \theta_{\mathbf{x}_{ij}}(1 - \theta_{\mathbf{x}_{ij}}).$$

Thus

$$\frac{\partial l_{ij}}{\partial \boldsymbol{\beta}} = \nu \theta_{\mathbf{x}_{ij}}(1 - \theta_{\mathbf{x}_{ij}})[\phi(\theta_{\mathbf{x}_{ij}}\nu + t_{ij}) - \phi((1 - \theta_{\mathbf{x}_{ij}})\nu + y_{ij} - t_{ij}) - \phi(\theta_{\mathbf{x}_{ij}}\nu) + \phi((1 - \theta_{\mathbf{x}_{ij}})\nu)]\mathbf{x}_{ij}.$$

The second derivative of l_{ij} w.r.t. $\boldsymbol{\beta}$ is

$$\frac{\partial^2 l_{ij}}{\partial \boldsymbol{\beta} \partial \boldsymbol{\beta}^\top} = \frac{\partial^2 l_{ij}}{\partial \theta_{\mathbf{x}_{ij}}^2} \cdot \left(\frac{\partial \theta_{\mathbf{x}_{ij}}}{\partial \eta_{ij}} \right)^2 \cdot \left(\frac{\partial \eta_{ij}}{\partial \boldsymbol{\beta}} \right) \left(\frac{\partial \eta_{ij}}{\partial \boldsymbol{\beta}^\top} \right) + \frac{\partial l_{ij}}{\partial \theta_{\mathbf{x}_{ij}}} \cdot \frac{\partial^2 \theta_{\mathbf{x}_{ij}}}{\partial \eta_{ij}^2} \cdot \left(\frac{\partial \eta_{ij}}{\partial \boldsymbol{\beta}} \right) \left(\frac{\partial \eta_{ij}}{\partial \boldsymbol{\beta}^\top} \right) + \frac{\partial l_{ij}}{\partial \theta_{\mathbf{x}_{ij}}} \cdot \frac{\partial \theta_{\mathbf{x}_{ij}}}{\partial \eta_{ij}} \frac{\partial^2 \eta_{ij}}{\partial \boldsymbol{\beta} \partial \boldsymbol{\beta}^\top}.$$

The third term on the right-hand side is equal to zero. With ψ being the trigamma function,

$$\frac{\partial^2 l_{ij}}{\partial \theta_{\mathbf{x}_{ij}}^2} = \nu^2 [\psi(\theta_{\mathbf{x}_{ij}}\nu + t_{ij}) + \psi((1 - \theta_{\mathbf{x}_{ij}})\nu + y_{ij} - t_{ij}) - \psi(\theta_{\mathbf{x}_{ij}}\nu) - \psi((1 - \theta_{\mathbf{x}_{ij}})\nu)].$$

Thus the first term is

$$\begin{aligned} & \frac{\partial^2 l_{ij}}{\partial \theta_{\mathbf{x}_{ij}}^2} \cdot \left(\frac{\partial \theta_{\mathbf{x}_{ij}}}{\partial \eta_{ij}} \right)^2 \cdot \left(\frac{\partial \eta_{ij}}{\partial \boldsymbol{\beta}} \right) \left(\frac{\partial \eta_{ij}}{\partial \boldsymbol{\beta}^\top} \right)^\top \\ &= \nu^2 [\psi(\theta_{\mathbf{x}_{ij}}\nu + t_{ij}) + \psi((1 - \theta_{\mathbf{x}_{ij}})\nu + y_{ij} - t_{ij}) - \psi(\theta_{\mathbf{x}_{ij}}\nu) - \psi((1 - \theta_{\mathbf{x}_{ij}})\nu)] \theta_{\mathbf{x}_{ij}}^2 (1 - \theta_{\mathbf{x}_{ij}})^2 \mathbf{x}_{ij} \mathbf{x}_{ij}^\top. \end{aligned}$$

The second term, which has expectation zero, is

$$\begin{aligned} & \frac{\partial l_{ij}}{\partial \theta_{\mathbf{x}_{ij}}} \cdot \frac{\partial^2 \theta_{\mathbf{x}_{ij}}}{\partial \eta_{ij}^2} \cdot \left(\frac{\partial \eta_{ij}}{\partial \boldsymbol{\beta}} \right) \left(\frac{\partial \eta_{ij}}{\partial \boldsymbol{\beta}^\top} \right)^\top \\ &= \nu [\phi(\theta_{\mathbf{x}_{ij}}\nu + t_{ij}) - \phi((1 - \theta_{\mathbf{x}_{ij}})\nu + y_{ij} - t_{ij}) - \phi(\theta_{\mathbf{x}_{ij}}\nu) + \phi((1 - \theta_{\mathbf{x}_{ij}})\nu)] \theta_{\mathbf{x}_{ij}} (1 - \theta_{\mathbf{x}_{ij}}) (1 - 2\theta_{\mathbf{x}_{ij}}) \mathbf{x}_{ij} \mathbf{x}_{ij}^\top. \end{aligned}$$

For each $i = 1, 2, j = 1, 2, \dots, n_i$, let

$$a_{ij} = \phi(\theta_{\mathbf{x}_{ij}}\nu + t_{ij}) - \phi((1 - \theta_{\mathbf{x}_{ij}})\nu + y_{ij} - t_{ij}) - \phi(\theta_{\mathbf{x}_{ij}}\nu) + \phi((1 - \theta_{\mathbf{x}_{ij}})\nu)$$

$$b_{ij} = \psi(\theta_{\mathbf{x}_{ij}}\nu + t_{ij}) + \psi((1 - \theta_{\mathbf{x}_{ij}})\nu + y_{ij} - t_{ij}) - \psi(\theta_{\mathbf{x}_{ij}}\nu) - \psi((1 - \theta_{\mathbf{x}_{ij}})\nu).$$

Since the total log likelihood is $l = \sum_{i,j} l_{ij}$,

$$\frac{\partial l}{\partial \boldsymbol{\beta}} = \nu \sum_{i,j} a_{ij} \theta_{\mathbf{x}_{ij}} (1 - \theta_{\mathbf{x}_{ij}}) \mathbf{x}_{ij} = \nu \mathbf{X}^\top W_1 \mathbf{z},$$

where the rows of \mathbf{X} are \mathbf{x}_{ij}^\top , $W_1 = \text{diag}(a_{ij})$ and $\mathbf{z} = (\theta_{\mathbf{x}_{11}}(1 - \theta_{\mathbf{x}_{11}}), \dots, \theta_{\mathbf{x}_{1n_1}}(1 - \theta_{\mathbf{x}_{1n_1}}), \dots, \theta_{\mathbf{x}_{2n_2}}(1 - \theta_{\mathbf{x}_{2n_2}}))^\top$. The rows of \mathbf{X}, W_1 and the elements of \mathbf{z} are ordered first by j and then i .

$$\begin{aligned} \frac{\partial^2 l}{\partial \boldsymbol{\beta} \partial \boldsymbol{\beta}^\top} &= \nu^2 \sum_{i,j} b_{ij} \theta_{\mathbf{x}_{ij}}^2 (1 - \theta_{\mathbf{x}_{ij}})^2 \mathbf{x}_{ij} \mathbf{x}_{ij}^\top + \nu \sum_{i,j} a_{ij} \theta_{\mathbf{x}_{ij}} (1 - \theta_{\mathbf{x}_{ij}}) (1 - 2\theta_{\mathbf{x}_{ij}}) \mathbf{x}_{ij} \mathbf{x}_{ij}^\top \\ &= -\nu \mathbf{X}^\top W_2 \mathbf{X}, \end{aligned}$$

where $W_2 = -\text{diag}(\nu b_{ij} \theta_{\mathbf{x}_{ij}}^2 (1 - \theta_{\mathbf{x}_{ij}})^2 + a_{ij} \theta_{\mathbf{x}_{ij}} (1 - \theta_{\mathbf{x}_{ij}}) (1 - 2\theta_{\mathbf{x}_{ij}}))$. The columns of W_2 is also ordered first by j and then by i .

When applying Laplace approximation to evaluate the marginal likelihood for a fixed ν ,

$$L_\nu = \int \exp\{l(\boldsymbol{\beta}) + \log \pi(\boldsymbol{\beta})\} d\boldsymbol{\beta},$$

where π is the prior on $\boldsymbol{\beta}$. For example, with $\pi(\boldsymbol{\beta})$ is the independent normal $N(0, \sigma_k^2)$ on the k -th element of $\boldsymbol{\beta}$, let $h_\nu(\boldsymbol{\beta}) = l(\boldsymbol{\beta}) + \log \pi(\boldsymbol{\beta}) = l(\boldsymbol{\beta}) - \boldsymbol{\beta}^\top \Sigma^{-1} \boldsymbol{\beta} / 2$, where $\Sigma = \text{diag}(\sigma_1^2, \dots, \sigma_d^2)$, we have

$$\begin{aligned} \frac{\partial h_\nu(\boldsymbol{\beta})}{\partial \boldsymbol{\beta}} &= \frac{\partial l}{\partial \boldsymbol{\beta}} - \Sigma^{-1} \boldsymbol{\beta} \\ \frac{\partial^2 h_\nu(\boldsymbol{\beta})}{\partial \boldsymbol{\beta} \partial \boldsymbol{\beta}^\top} &= \frac{\partial^2 l}{\partial \boldsymbol{\beta} \partial \boldsymbol{\beta}^\top} - \Sigma^{-1}. \end{aligned}$$

Hence the Newton-Raphson step for solving the MLE of β given ν is given by

$$\hat{\beta}^{(t+1)} = \hat{\beta}^{(t)} + \left(\mathbf{X}^\top W_2^{(t)} \mathbf{X} + \Sigma^{-1}/\nu \right)^{-1} \left(\mathbf{X}^\top W_1^{(t)} \mathbf{z}^{(t)} - \Sigma^{-1} \hat{\beta}^{(t)}/\nu \right).$$

Under the alternative, suppose that $\pi(\beta) = \pi(\beta_1)\pi(\gamma)$, where β_1 are the coefficients for the covariates and γ for the group indicator. Instead of using independent normal prior on γ , the LIM g -prior (Li and Clyde, 2015) could be adopted. Using the independent normal prior for β_1 , we have

$$\begin{aligned} h_\nu(\beta) &= l(\beta) + \log \pi(\beta) \\ &= l(\beta) - \beta_1^\top \Sigma^{-1} \beta_1 / 2 - g^{-1} \mathcal{J}_\nu(\hat{\gamma}) \gamma^2 / 2 \\ &= l(\beta) - \beta_1^\top \Sigma^{-1} \beta_1 / 2 - g^{-1} \nu (\mathbf{X}^\top \hat{W}_2 \mathbf{X})_2 \gamma / 2 \end{aligned}$$

where $(\mathbf{X}^\top \hat{W}_2 \mathbf{X})_2$ denote the block of the Hessian matrix corresponding to γ . Therefore,

$$\begin{aligned} \frac{\partial h_\nu(\beta)}{\partial \beta} &= \nu \mathbf{X}^\top W_1 \mathbf{z} - \begin{pmatrix} \Sigma^{-1} \beta_1 \\ g^{-1} \nu (\mathbf{X}^\top \hat{W}_2 \mathbf{X})_2 \gamma \end{pmatrix} \\ \frac{\partial^2 h_\nu(\beta)}{\partial \beta \partial \beta^\top} &= -\nu \mathbf{X}^\top W_2 \mathbf{X} - \begin{pmatrix} \Sigma^{-1} & \mathbf{0} \\ \mathbf{0} & g^{-1} \nu (\mathbf{X}^\top \hat{W}_2 \mathbf{X})_2 \end{pmatrix}. \end{aligned}$$

The resulting NR update is

$$\begin{aligned} \hat{\beta}^{(t+1)} &= \hat{\beta}^{(t)} + \left(\mathbf{X}^\top W_2^{(t)} \mathbf{X} + \begin{pmatrix} \Sigma^{-1}/\nu & \mathbf{0} \\ \mathbf{0} & g^{-1} (\mathbf{X}^\top W_2^{(t)} \mathbf{X})_2 \end{pmatrix} \right)^{-1} \\ &\quad \times \left(\mathbf{X}^\top W_1^{(t)} \mathbf{z}^{(t)} - \begin{pmatrix} \hat{\Sigma}^{-1} \beta_1^{(t)}/\nu \\ g^{-1} (\mathbf{X}^\top W_2^{(t)} \mathbf{X})_2 \hat{\gamma}^{(t)} \end{pmatrix} \right). \end{aligned}$$

B Additional figures

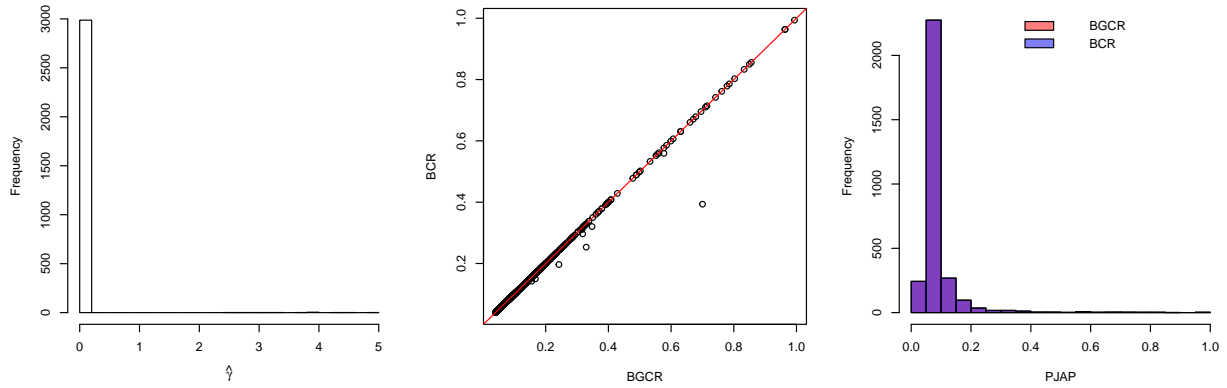


Figure S1: BGCR vs BCR under the null in scenario 3. Left: Histogram of the estimated $\hat{\gamma}$ in BGCR; Middle: PJAPs of BGCR vs BCR; Right: Histograms of the PJAPs of BGCR and BCR.

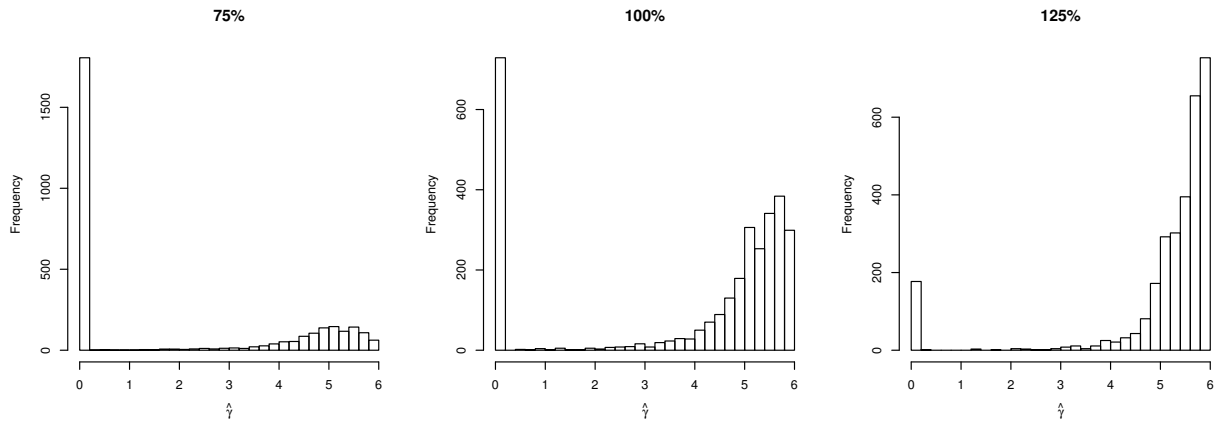


Figure S2: Estimated $\hat{\gamma}$ under the alternatives in scenario 3.

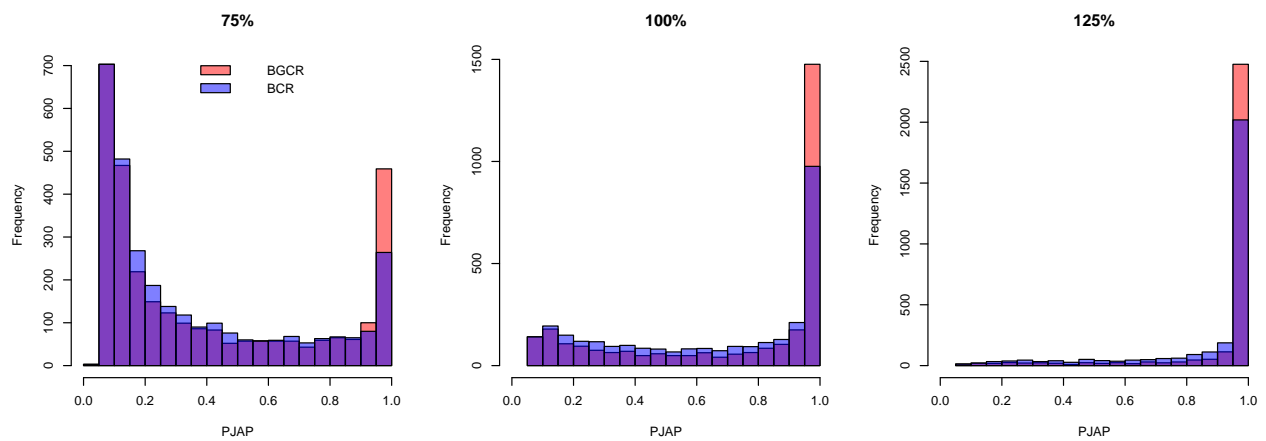


Figure S3: Histograms of the PJAPs under the alternatives in scenario 3.

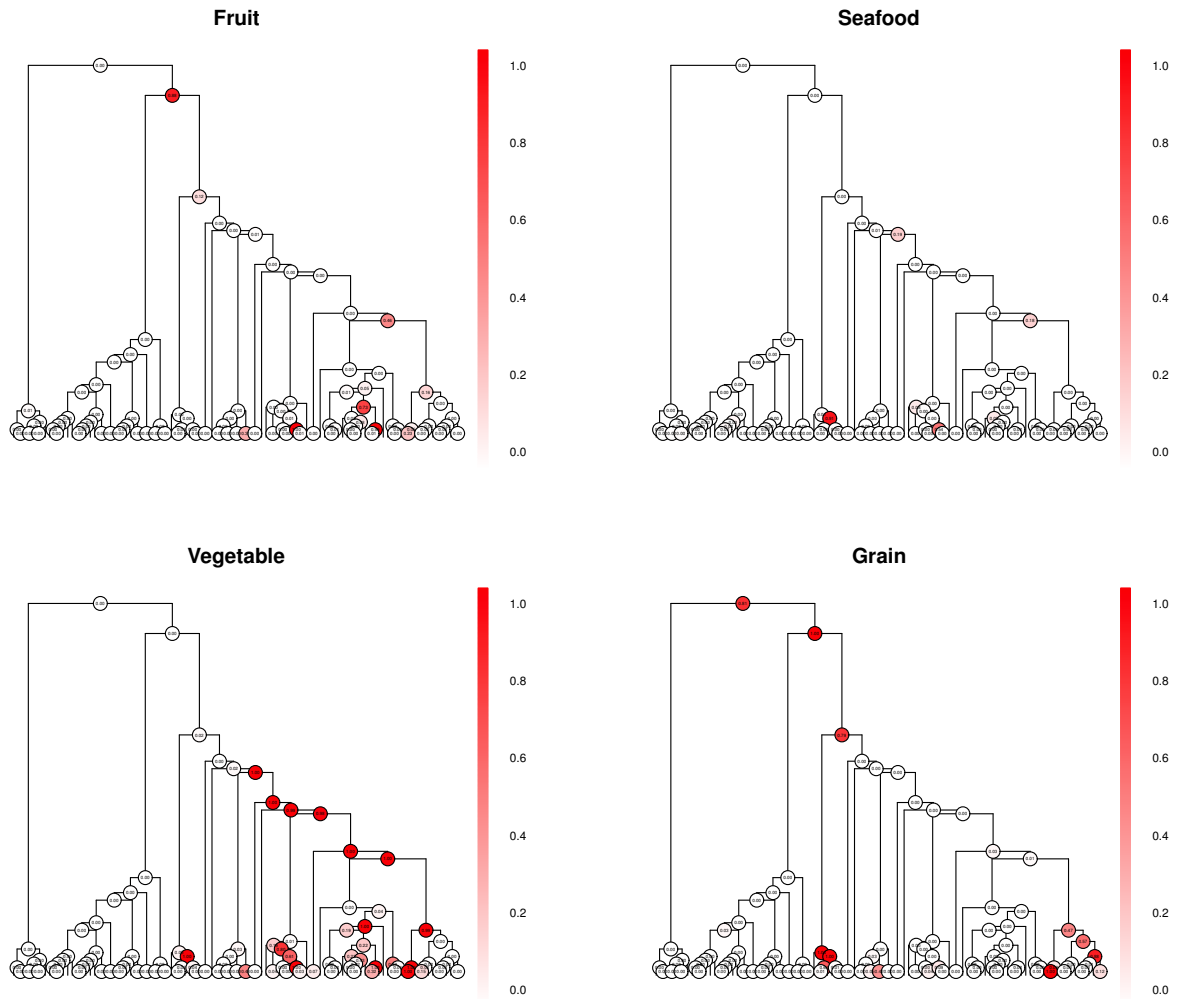


Figure S4: PMAPs for the grouping diets with rejected global null when no covariate is adjusted.

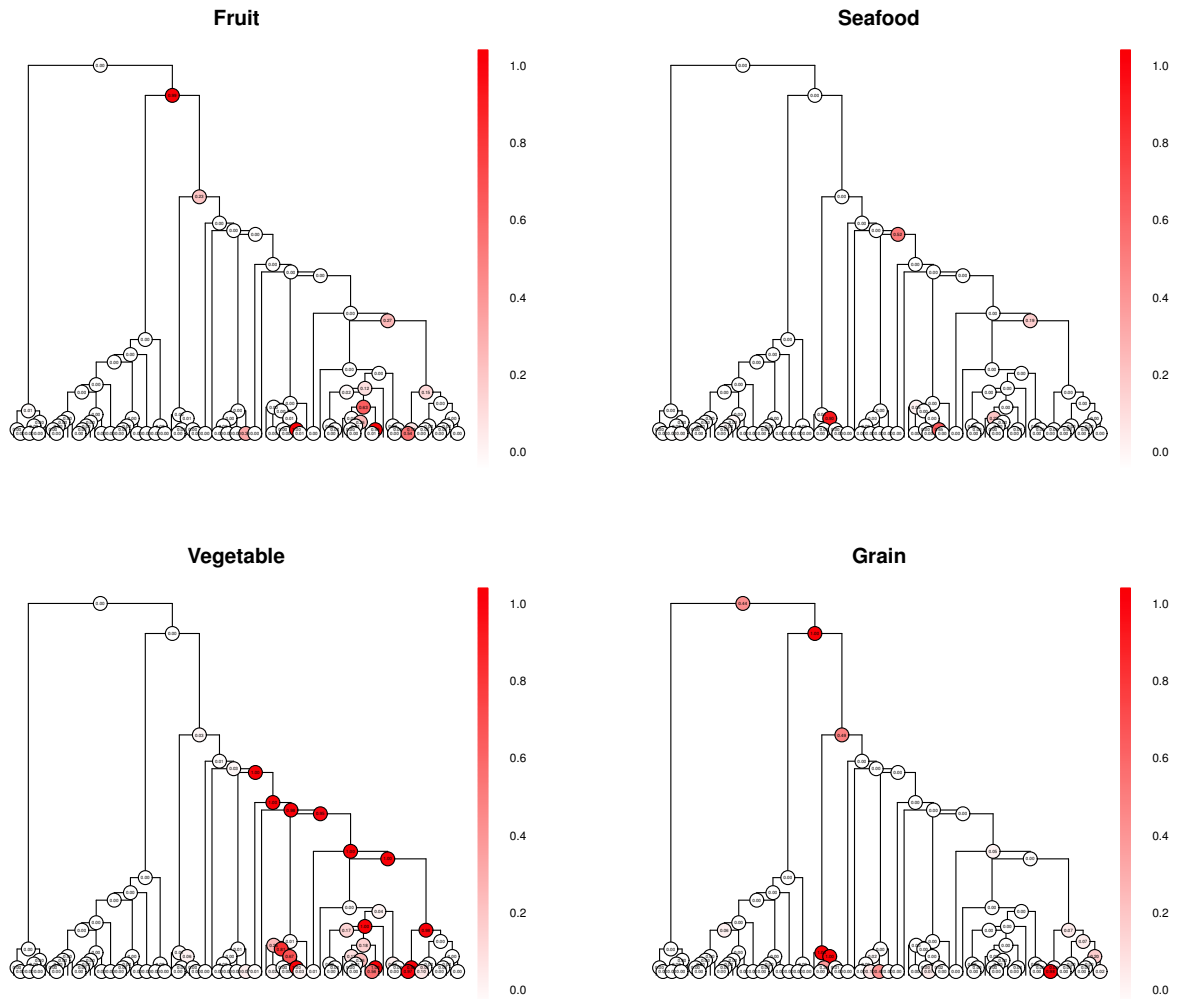


Figure S5: PMAPs for the grouping diets with rejected global null when only the non-dietary covariates are adjusted.